Research Paper

GEOSPHERE

GEOSPHERE; v. 14, no. 4

doi:10.1130/GES01618.1

14 figures

CORRESPONDENCE: eehlb@leeds.ac.uk

CITATION: Brooks, H.L., Hodgson, D.M., Brunt, R.L., Peakall, J., Poyatos-Moré, M., and Flint, S.S., 2018, Disconnected submarine lobes as a record of stepped slope evolution over multiple sea-level cycles: Geosphere, v. 14, no. 4, https://doi.org/10.1130/GES01618.1.

Science Editor: Shanaka de Silva
Associate Editor: Andrea Fildani

Received 3 October 2017
Revision received 22 February 2018
Accepted 24 April 2018

Disconnected submarine lobes as a record of stepped slope evolution over multiple sea-level cycles

Hannah L. Brooks[1], David M. Hodgson[1], Rufus L. Brunt[2], Jeff Peakall[1], Miquel Poyatos-Moré[2,3], and Stephen S. Flint[2]

[1]Stratigraphy Group, School of Earth and Environment, University of Leeds, Leeds LS2 9JT, UK
[2]Stratigraphy Group, School of Earth and Environmental Sciences, University of Manchester, Manchester, M13 9PL, UK
[3]Department of Geosciences, University of Oslo, 0371 Oslo, Norway

ABSTRACT

The effects of abrupt changes in slope angle and orientation on turbidity current behavior have been investigated in numerous physical and numerical experiments and examined in outcrop, subsurface, and modern systems. However, the long-term impact of subtle and evolving seabed topography on the stratigraphic architecture of deep-water systems requires fine-scale observations and extensive 3-D constraints. This study focuses on the Permian Laingsburg and Fort Brown formations, where multiple large sand-rich systems (Units A–F) have been mapped from entrenched slope valleys, through channel-levee systems, to basin-floor lobe complexes over a 2500 km² area. Here, we investigate three thinner (typically <5 m in thickness) and less extensive sand-rich packages, Units A/B, B/C, and D/E, between the large-scale systems. Typically, these sand-rich units are sharp-based and topped, and contain scours and mudstone clast conglomerates that indicate deposition from high-energy turbidity currents. The mapped thickness and facies distribution suggest a lobate form. These distinctive units were deposited in similar spatial positions within the basin-fill and suggest similar accommodation patterns on the slope and basin floor prior to the larger systems (B, C, and E). Stratigraphically, these thin units represent the first sand deposition following major periods of shut-down in sediment supply, and are interpreted as marking a partial re-establishment of sand delivery pathways creating "disconnected lobes" that are fed mainly by flows sourced from failures on the shelf and upper slope rather than major feeder channel-levee systems.

Thickness and facies patterns throughout the deep-water stratigraphy suggest seabed topography was present early in the basin formation and maintained persistently in a similar area to ultimately form a stepped slope profile. The stepped slope profile evolved through three key stages of development: Phase 1, where sediment supply exceeds deformation rate (likely caused by differential subsidence); Phase 2, where sediment supply is on average equal to deformation rate; and Phase 3, where deformation rate outpaces sediment supply. This study demonstrates that smaller systems are a sensitive record of evolving seabed topography and they can consequently be used to recreate more accurate paleotopographic profiles.

INTRODUCTION

Topographic complexity across submarine slopes varies both spatially and temporally (Fig. 1). Topography can include three-dimensional confinement of ponded mini-basins (e.g., Prather et al., 1998, 2012a, 2012b, 2017; Badalini et al., 2000; Winker and Booth, 2000; Sinclair and Tomasso, 2002; Shultz and Hubbard, 2005; Sylvester et al., 2015); barriers creating tortuous corridors (e.g., Smith, 2004a; Hay, 2012); and more subtle gradient changes (generally <1° to few degrees) of stepped slope profiles (Figs. 1B and 1C), which create higher gradient ramps linking lower gradient steps (e.g., O'Byrne et al., 2004; Smith, 2004a; Barton, 2012; Deptuck et al., 2012; Hay, 2012). High-amplitude seabed topography and associated major gradient changes have been well documented in seismic reflection data sets of modern systems, such as in the Gulf of Mexico (Prather et al., 1998, 2017; Fig. 1D), the Western Niger Delta slope (Jobe et al., 2017; Fig 1E), offshore Norway (Jackson et al., 2008) and offshore Angola (Hay, 2012), as well as in outcrop studies, including the Castagnola Formation (4–12°; Felletti, 2002; Southern et al., 2015; Marini et al., 2016); the Laga Formation (6–8°; Marini et al., 2015); and the Grès d'Annot (4–10°; Amy et al., 2007; Salles et al., 2014).

While the effects of high-gradient stepped slopes on deposition processes and architecture have been examined, the impact of subtle gradient changes on sediment distribution and flow pathways is less clear. Subtle gradient changes having a profound impact on flow processes and therefore configuration of deep-water systems have been shown from experimental (Baines, 1984; Edwards et al., 1994; Kneller and McCaffrey, 1999; Kneller and Buckee, 2000; Nasr-Azadani and Meiburg, 2014), outcrop (e.g., Kane et al., 2010; Patacci et al., 2014), and modern seabed data sets (e.g., Stevenson et al., 2013, 2014; e.g. Kneller, 1995). Despite this, previous outcrop studies on the effects of subtle fixed and dynamic topography are limited in their spatial and temporal extent (e.g., Smith, 2004b; Spychala et al., 2017a), and the influence of seabed topography over multiple depositional cycles remains unknown. Studies using seismic reflection data sets can show evolution over multiple stages of deposition (e.g., Beaubouef and Abreu, 2006; Mayall et al., 2010; Hay, 2012; Jobe et al., 2017), but they generally focus on complicated topographic

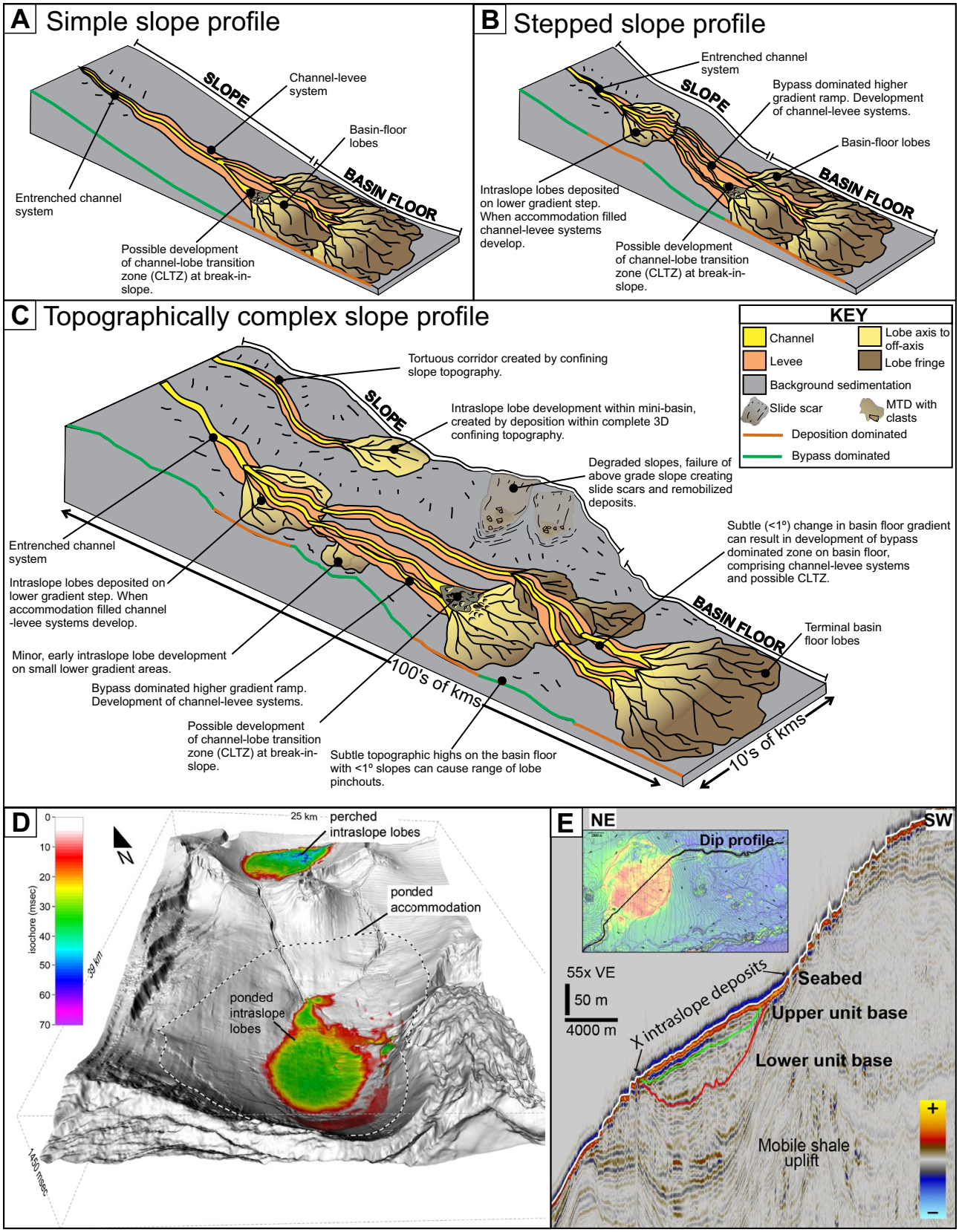

Figure 1. Examples of slope and basin-floor topography and resultant deposits. (A) Simple slope profile with single break-in-slope changing from bypass dominated channel-levee system to depositional dominated basin-floor lobes, with potential for channel-lobe transition zone (CLTZ) development at base-of-slope. (B) Stepped slope profile with higher gradient ramps linking lower gradient steps. Formation of entrenched channel/channel levee systems on ramps and intraslope/basin-floor lobes on steps, with potential for CLTZ development at breaks-of-slope. (C) Topographically complex slope, encompassing varying magnitudes of topography. Development of several ramps within entrenched channel/channel levee systems, including a step on the basin floor. Intraslope and basin-floor lobe development on lower gradient steps. Formation of high magnitude topography leads to the creation of a tortuous corridor controlling channel levee systems, and development of mini-basins where 3-D closure occurs. Topography on slopes is generally of much greater magnitude than on the basin floor. MTD—mass transport deposit. (D) Perspective view of partially (perched) and fully (ponded) confined intraslope deposits from the Brazos-Trinity intraslope basins, Gulf of Mexico, linked by a higher gradient area dominated by sediment bypass (modified and republished with permission of John Wiley and Sons, Inc., from *Basin Research*, Prather et al., vol. 29, issue 3, 2017; permission conveyed through Copyright Clearance Center, Inc.). (E) Thickness map and dip seismic profile of intraslope basin fill from the Western Niger Delta slope, demonstrating the formation and healing of intraslope accommodation above mobile shale (modified from *GSA Bulletin*, Jobe et al., vol. 129, 2017; cropped image with minor changes to text).

templates, such as tortuous corridors (Smith, 2004a; Hay, 2012), mini-basins (Booth et al., 2003; Beaubouef and Abreu, 2006; Madof et al., 2009; Pirmez et al., 2012; Prather et al., 2012b; Oluboyo et al., 2014; Doughty-Jones et al., 2017), and piggy-back basins/foredeep margin slopes (Covault et al., 2009), and/or do not span multiple large-scale sea-level cycles (e.g., Beaubouef and Abreu, 2006; Barton, 2012). Moreover, these studies do not investigate the long-term stratigraphic evolution of slopes nor characterize stratigraphic architecture at a scale that resolves relationships between sedimentary processes and seabed topography.

This study characterizes three thin (<15 m) sandstone bodies (Units A/B, B/C, and D/E) from the Permian Laingsburg and Fort Brown formations in the Karoo Basin, South Africa. These units differ greatly in sedimentology and architecture from the larger underlying and overlying slope and basin-floor systems (Units A–F) as their accumulation did not significantly modify the slope basin-floor profile during formation. Therefore, their utility as subtle topographic indicators is investigated, building on a stratigraphic framework established from previous studies. Objectives are: (*i*) to document influence of seabed topography through spatial variability in thickness and facies trends; (*ii*) to understand the sedimentary processes and depositional environments of Units A/B, B/C, and D/E; (*iii*) to investigate how and when seabed topography formed and evolved, and how this topography influenced deposition of larger Units C, D, E, and F; and (*iv*) to develop a model for stepped slope profile evolution over multiple successive sea-level cycles. This investigation will therefore further contribute to the understanding of subtle slope evolution and its varying influence on deep-water system facies and architecture at bed to system scale.

GEOLOGICAL BACKGROUND

Geology of the Karoo Basin

The Karoo Basin, South Africa (Fig. 2), has been previously interpreted as a retroarc foreland basin (Visser and Prackelt, 1996; Visser, 1997; Catuneanu et al., 1998), and more recently as a thermal sag basin in the Permian that evolved into a retroarc foreland basin in the Triassic (Tankard et al., 2009). The 8-km-thick Karoo Supergroup (Fig. 2C) is subdivided into the Dwyka, Ecca, and Beaufort groups. The Dwyka Group comprises glacial deposits (Late Carboniferous to Early Permian); the Ecca Group clastic marine deposits (Permian); and the Beaufort fluvial deposits (Permian to Triassic; Belica et al., 2017). Basal deposits of the Lower Ecca Group (Fig. 2C) comprise the Prince Albert, Whitehill, and Collingham formations, mapped for 800 km along the southern margin of the Karoo Basin (Viljoen, 1992, 1994; Visser, 1992; Johnson et al., 1997). In the Laingsburg depocenter, the Collingham Formation is overlain by the Vischkuil Formation, forming the basal section of the 1800-m-thick progradational succession from basin-floor deposits (Vischkuil and Laingsburg formations; Sixsmith et al., 2004; Van der Merwe et al., 2010), through a channelized submarine slope (Fort Brown Formation; Hodgson et al., 2011; Di Celma et al., 2011; Flint et al., 2011) to shelf-edge and shelf deltas (Waterford Formation; Jones et al., 2015; Poyatos-Moré et al., 2016). Regional paleoflow is toward the northeast and east throughout the succession with the main deep-water sediment entry point located to the southwest (Van der Merwe et al., 2014). Regional-scale mapping of successive slope to basin-floor systems (Units D–F) in the Laingsburg depocenter indicates the presence of a confining, lateral basin margin to the south of the depocenter, oriented east-to-west (Van der Merwe et al., 2014; Brooks et al., 2018b).

The Laingsburg and Fort Brown Formations

The Laingsburg Formation comprises the stratigraphic Units A, A/B, and B, and the Fort Brown Formation, Units B/C, C, D, D/E, E, F, and G (Fig. 2C; Flint et al., 2011). This study examines Units A–F, and represents the first detailed study on the less extensive, thinner Units A/B, B/C, and D/E (Fig. 2C), that are exposed along a series of E-W–oriented subparallel post-depositional fold limbs (Fig. 2B), and intersected in a number of cored research boreholes. Detailed mapping and physical correlation of all units utilizes a regional stratigraphic framework established from previous studies (Grecula et al., 2003; Figueiredo et al., 2010, 2013; Di Celma et al., 2011; Flint et al., 2011; Hodgson et al., 2011; Kane and Hodgson, 2011; Brunt et al., 2013a, 2013b; Morris et al., 2014a, 2014b, 2016; Van der Merwe et al., 2014; Spychala et al., 2015, 2017a; Brooks et al., 2018b). The Laingsburg and Fort Brown formations have been divided into four composite sequence sets, the first comprising Unit A, the second Units A/B and B, the third Units B/C, C, and D; and the fourth Units D/E, E, and F (Flint et al., 2011). Units C, D, E, and F each represents a lowstand sequence set, with an overlying 10–30-m-thick regional hemipelagic mudstone representing the corresponding transgressive/highstand sequence set (Flint et al., 2011). Lowstand sequence sets can be further subdivided into separate depositional sequences, including a sand-rich lowstand systems tract (LST; represented stratigraphically by a subunit, e.g., E1, E2, or E3) and an overlying transgressive/highstand systems tract mudstone (~1–5 m thick) (Figueiredo et al., 2010, 2013; Di Celma et al., 2011; Hodgson et al., 2011).

Regional mapping and correlation of units C to F have demonstrated an architectural change from sand-attached (Units C and D) to sand-detached channel-lobe transition zones (Units E and F; Van der Merwe et al., 2014; Brooks et al., 2018b). The recognition of intraslope lobes in Units D/E, E, and F (Figueiredo et al., 2010; Spychala et al., 2015), and coarse-grained bypass-dominated zones, consisting of thin channel-levee deposits and channel-lobe transition zones (sensu Mutti, 1995; Van der Merwe et al., 2014; Brooks et al., 2018b) supports the presence of a stepped slope profile at the time of E and F deposition (e.g., Figs. 1B and 1C; Van der Merwe et al., 2014; Brooks et al., 2018b). This paper focuses on the sedimentology and stratigraphic architecture of the thinner units (A/B, B/C, and D/E) in order to decipher the origin and

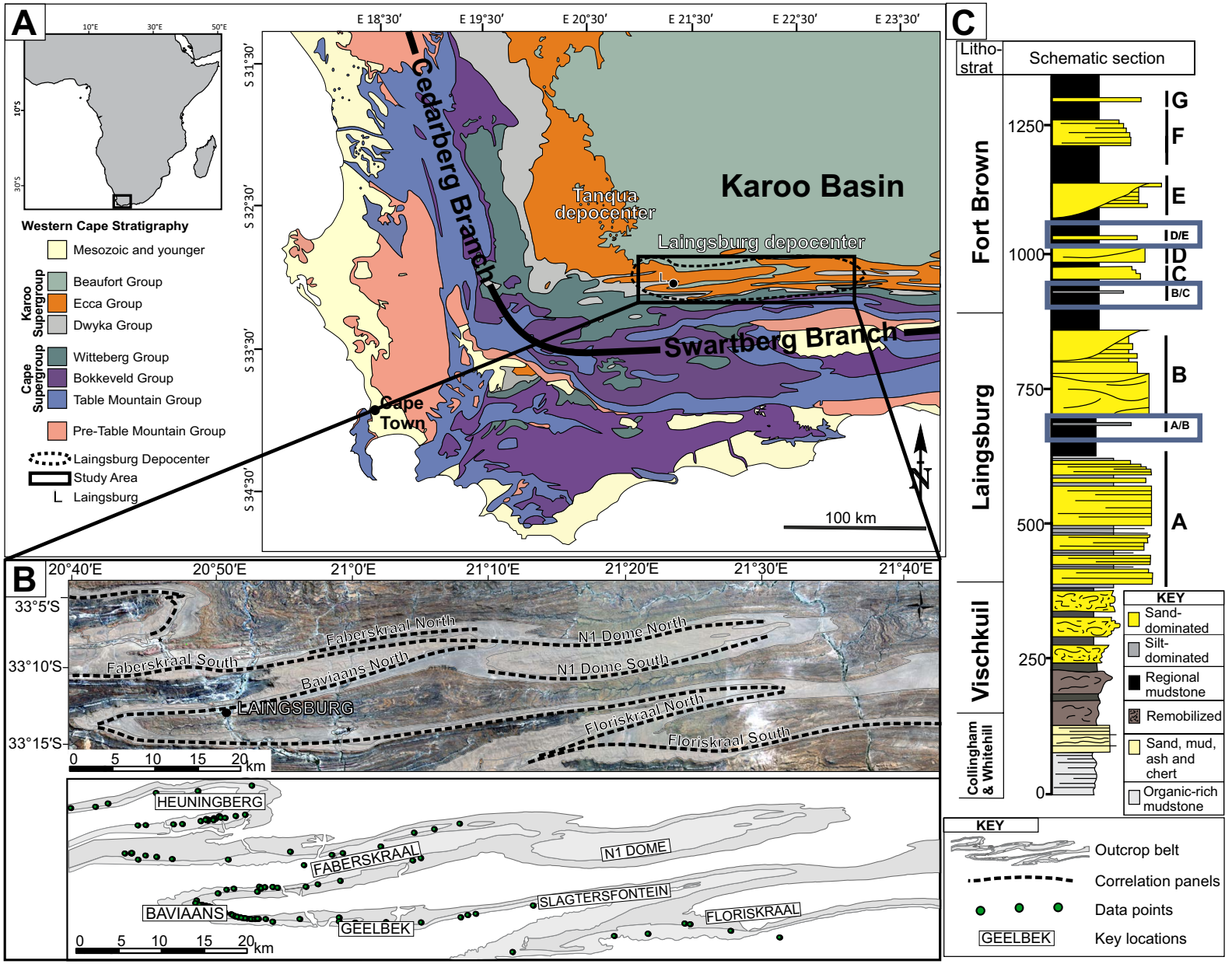

Figure 2. (A) Map of Africa and geological map of SW Africa with location of Laingsburg depocenter. (B) Enlarged map of Laingsburg depocenter showing location of outcrop belts along post-depositional fold limbs, simplified map showing outcrop belt, datapoints used in this study and key locations. Black dashed lines highlight the regional scale correlation panels. (C) Stratigraphic column of Ecca group stratigraphy, highlighting submarine fan Units A, B, C, D, E, F, and G as well as discontinuous smaller fan Units A/B, B/C, and D/E in the Laingsburg and Fort Brown formations.

presence of fixed and dynamic slope topography throughout the deposition of the Laingsburg and Fort Brown formations, that resulted in the formation of a stepped slope profile (Van der Merwe et al., 2014; Brooks et al., 2018b).

METHODOLOGY

Over 100 stratigraphic sections were measured and logged at the mm–cm scale, to characterize the range of sedimentary facies of Units A/B, B/C, and D/E and build thickness and paleogeographic maps of each unit over tens of kilometers in depositional dip and strike. Sedimentary logs document lithology, grain size, sedimentary structures, and stratal boundaries. Beds with similar thickness, grain size, and sedimentary structures are grouped into facies. Facies are used to interpret environments of deposition within the context of extensive paleoenvironmental reconstructions already undertaken in the Laingsburg depocenter (e.g., Grecula et al., 2003; Figueiredo et al., 2010, 2013; Di Celma et al., 2011; Flint et al., 2011; Van der Merwe et al., 2014; Spychala et al., 2015, 2017a, 2017b; Brooks et al., 2018b). A physical correlation framework was established by walking out stratigraphic surfaces between sections.

Thickness distributions were created by fitting a surface to values obtained from logged sections using the kriging tool within the ArcGIS® Geostatistical Wizard. Maps are extended beyond extremities of the input data by the surfacing algorithm, with unrealistic values removed and observed trends applied. Paleogeographic maps utilize data from previous studies in the Karoo (Grecula et al., 2003; Figueiredo et al., 2010, 2013; Di Celma et al., 2011; Flint et al., 2011; Van der Merwe et al., 2014; Spychala et al., 2015, 2017a, 2017b; Brooks et al., 2018b) and represent gross depositional environments for each study interval. Unit C, D, E, and F paleogeographic maps are modified from Van der Merwe et al. (2014) incorporating data from Spychala et al. (2015) and Brooks et al. (2018b). Flow trends within the paleogeographic maps are based on restored paleocurrent data collected from ripple laminations, flutes, grooves and scours.

A 3-D datacube was constructed in Petrel® by importing 100 composite logs from outcrop and six well logs consisting of the complete Whitehill Formation to Waterford Formation stratigraphy, with the Whitehill Formation used as a basal datum. Tops and bases of key lithostratigraphic units were selected using the well top function, and regional panels were used to interpret polylines to add datapoints between outcrop logs. Depth structure maps were constructed for each key surface using the "make a surface" function and cumulative thickness maps were created between key surfaces. Post-depositional tectonic shortening was corrected by stretching 13% in the Y direction, according to a mean value for palinspastic restoration derived by Spikings et al. (2015).

RESULTS

Seven distinct facies are described and interpreted in terms of sedimentary processes for Units A/B, B/C, and D/E (Figs. 3 and 4).

Structureless Sandstone Facies

Description

Structureless sandstone beds are fine grained, thin to thick bedded (0.1–1 m thick) with common dish and pillar structures, and weak normal grading at bed tops (Fig. 3A). Bed geometries are tabular with erosional bases, flutes, grooves, and other tool marks (Fig. 3B). Discontinuous mudstone-clast layers are often observed at bed amalgamation surfaces, bed bases, and dispersed within beds, with sub-angular to sub-rounded clasts (<15% clasts by volume, 0.1–10 cm A-axis; Figs. 3C, 4L, and 4M). Loading and flame structures are also common at amalgamated bed contacts. Basal beds are observed to thicken and thin over meters to 100s of meters, pinching out, infilling scoured sections and onlapping or downlapping onto underlying mudstone (Figs. 5 and 6). Beds occur in packages up to 14 m in thickness, but are generally <5 m thick (Fig. 6). Bioturbation fabric (mainly *Planolites*) is rarely observed at bed bases.

Interpretation

Structureless and weakly normally graded sandstone beds suggest deposition from sand-rich high-density turbidity currents (Bouma, 1962; Lowe, 1982; Mutti, 1992; Kneller and Branney, 1995). Lack of sedimentary structures suggests rapid deposition preventing any bedform development. The presence of dispersed rip-up clasts and mudstone clast-rich amalgamated contacts suggest long-lived erosion and progressive aggradation of deposits formed by depletive steady high-density flows (Kneller and Branney, 1995). Loading and dewatering structures form syn- and post-depositionally as a result of sediment liquefaction (Mulder and Alexander, 2001; Stow and Johansson, 2000).

Structured Sandstone Facies

Description

Structured sandstone beds are very fine to fine grained (0.05–1 m thick) with structures primarily consisting of ripple and climbing ripple cross lamination (Figs. 3F, 3H, and 4E) but also including planar lamination (Figs. 3D, 3E, and 4J) and dewatering structures (load casts and flames, and dish and pillar) (Figs. 3G, 4D, and 4F). Climbing ripple lamination can exhibit a high angle of climb (15–30°) with stoss-side preservation of laminae, which are locally sheared and overturned toward the bed top. Ripple cross-laminae can be heterolithic, comprised of both sandstone and siltstone, and mm–cm scale mud clasts (Fig. 3F). Beds occur in packages up to several meters thick (Fig. 3E). Bed geometries range from tabular to lenticular, draping surfaces as discontinuous depositional features, or as remnant erosional features that can form multiple

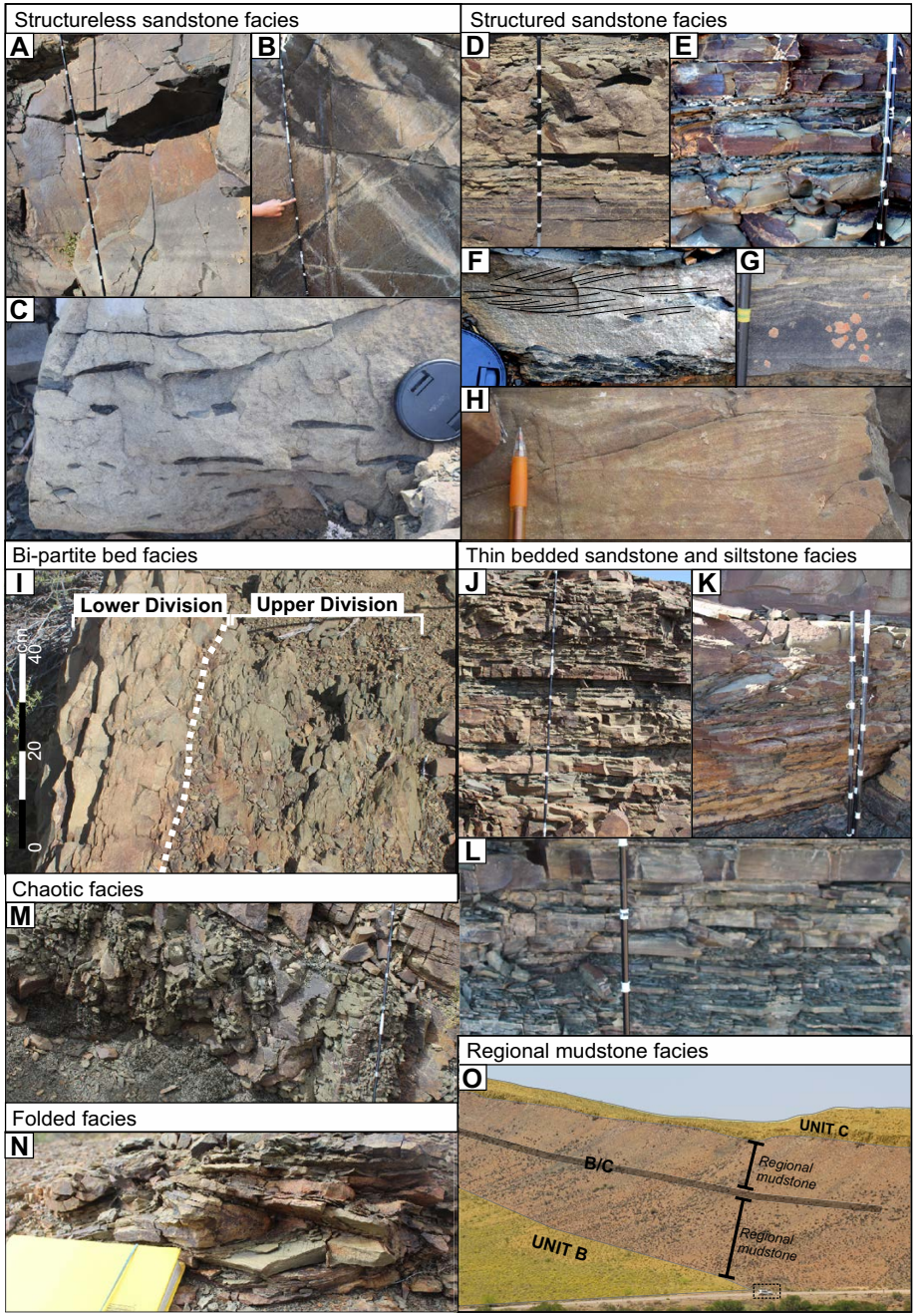

Figure 3. Representative photographs depicting facies present throughout the outcrop. (A) Thick structureless amalgamated sandstone. (B) Base of structureless sandstone bed showing grooves and tool marks. (C) Elongated mudstone clasts present near the base of a structureless sandstone bed. Lens cap is 7 cm in diameter. (D) Laminated and graded tops of structured sandstone beds. (E) Planar/ripple laminated very fine sandstone-siltstone beds. (F) Climbing ripple laminated sandstone bed, with mudclasts draping laminations and forming a layer at the base of the bed. Lens cap is 7 cm in diameter. (G) Dewatered banded sandstone. (H) Ripple laminated sandstone. Section of pencil is 7 cm in length. (I) Bipartite bed with lower division of fine sandstone and upper division of poorly sorted sandstone and siltstone with mm-cm–thick mudstone clasts and organic matter. (J) Interbedded 10–15 cm sandstone beds and thinner siltstone beds. (K) Interbedded sandstone and siltstone with deformation. (L) Interbedded cm-thick siltstone beds, overlain by thicker structured sandstone beds. (M) Debrite with mm-cm–scale mudclasts and organic fragments. (N) Tightly folded sandstone and siltstone thin beds, resulting from soft sediment deformation; notebook 15 cm in length. (O) Tens-of-m–thick mudstone packages separating larger and smaller fan units. Car for scale is marked by dashed box.

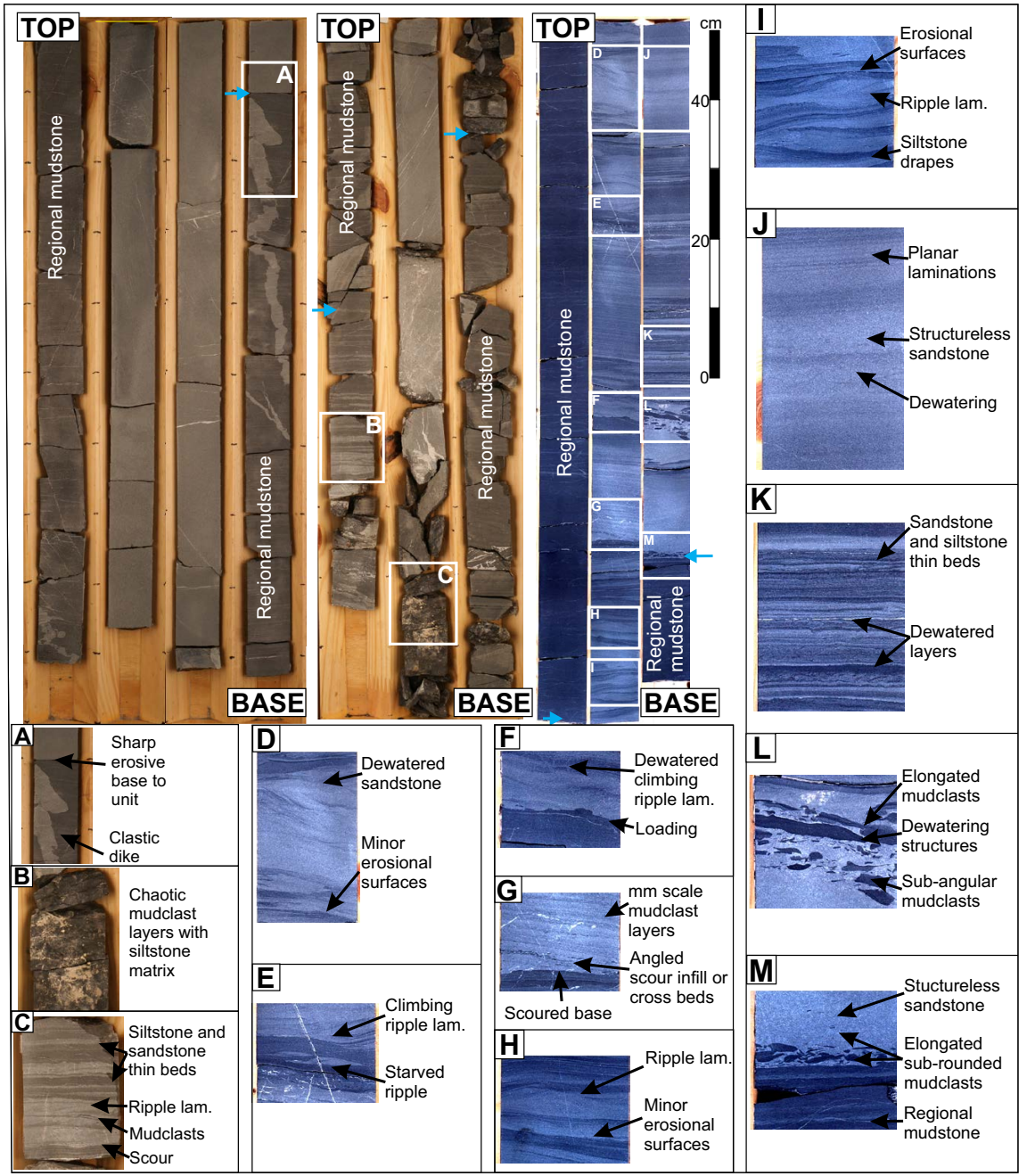

Figure 4. Core examples of Unit A/B (right) and B/C (left and center) demonstrating key features and range of structures recognized, including: sharp base and top of units; clastic injectites surrounding unit; mudclast layers throughout unit and mudclast conglomerates; ripple laminated sandstone and siltstone; planar laminated sandstone and siltstone; dewatering structures and small scale scouring. Blue arrows indicate top and base of units. Color and hue modified from original to accentuate structures.

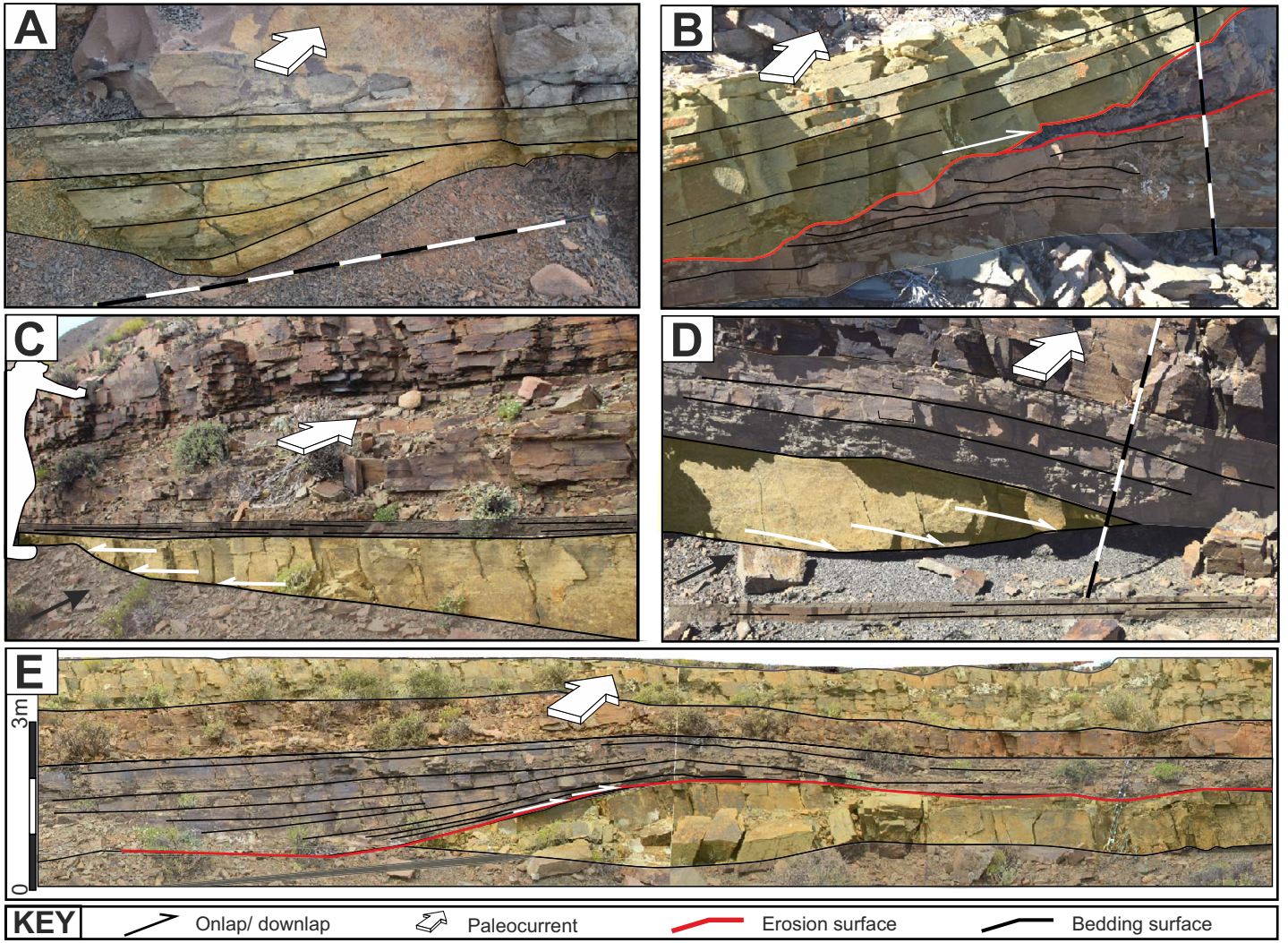

Figure 5. Range of discontinuous beds within A/B, B/C, and D/E. (A) Basal scour with draped infilling sandstone and siltstone. (B) Erosional surface cutting 1–2 m within unit truncating strata, with onlap of overlying beds. (C) Onlap of basal beds onto topography created by scouring or regional mudstone topography. (D) Downlap of basal beds onto regional mudstone. (E) Erosion surface within unit cutting down to base. Infilling beds onlap, and then drape over surface. Scale in A, B, and D indicates 10 cm intervals.

stacked packages. Packages can stack to form thin (<3 m) and wide (>100 m) sandstone units discussed further below. Within these packages, the basal beds thicken and thin over 10s to 100s of meters, pinching out and onlapping/downlapping on to underlying mudstone unit laterally and frontally (Fig. 5). Bioturbation, mainly *Planolites*, is rarely observed at bed tops and bases.

Interpretation

Climbing ripples form from continuous bedload traction under highly depositional flows. High angle of climb, with stoss-side preservation indicates high rates of aggradation (e.g., Allen, 1970; Jobe et al., 2012; Morris et al.,

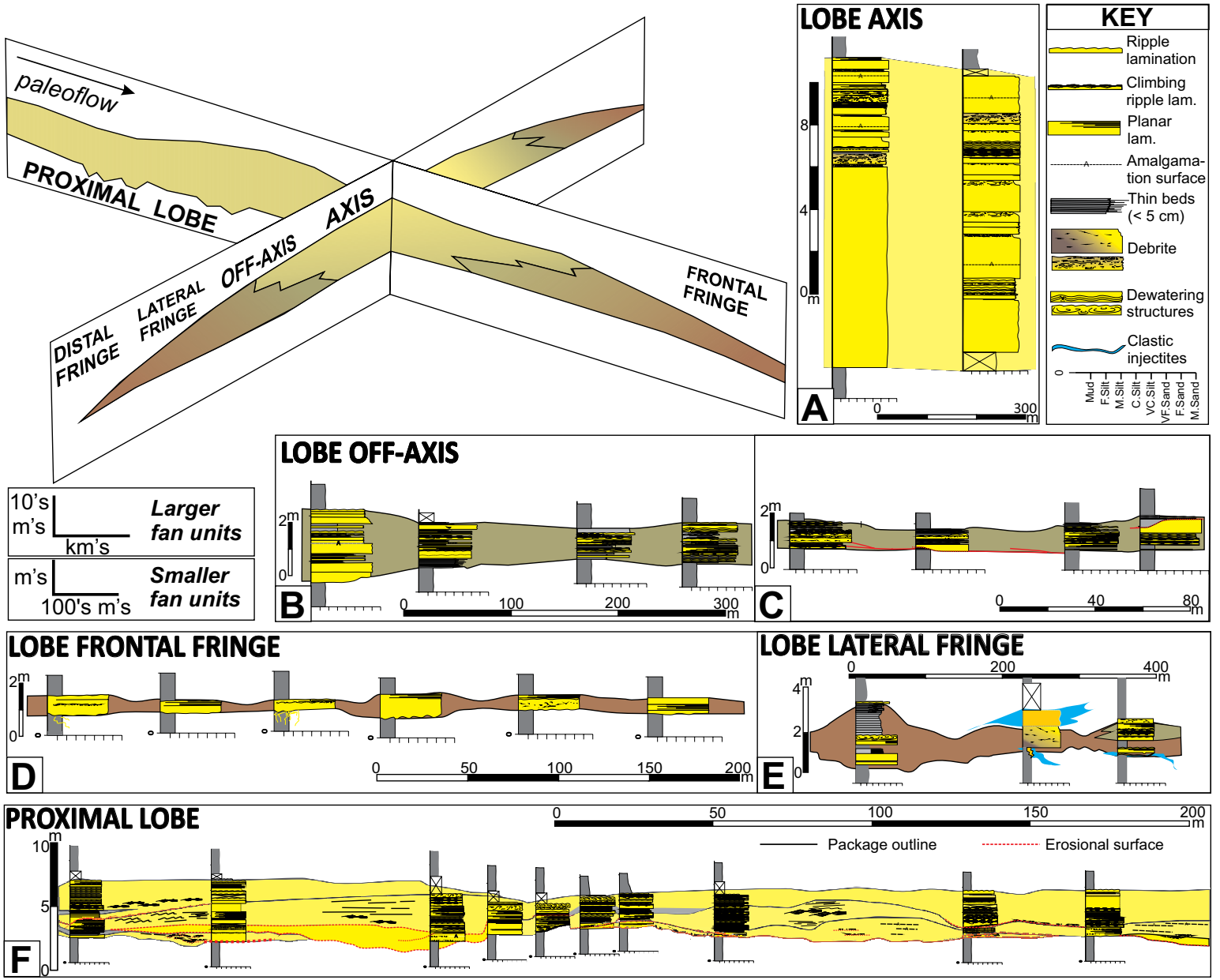

Figure 6. Key architectural elements recognized in Units A/B, B/C, and D/E. Sketch of 3-D lobe shows divisions of sub-environments, with scale demonstrating general thickness of smaller and larger fan units. (A) Lobe axis, (B and C) lobe off-axis, (D) lobe frontal fringe, (E) lobe lateral fringe, and (F) proximal lobe panels show representative section from Units A/B, B/C, and D/E. Blue indicates interpretation as clastic injectite (following criteria of Cobain et al., 2015). Locations of sections shown on Figure 7.

2014a, 2014b), commonly associated with non-uniformity in flows and accompanying decrease in velocity and/or flow height, possibly linked to an abrupt decrease in gradient or loss of confinement (e.g., Jobe et al., 2012; Morris et al., 2014a, 2014b), driving deposition through a reduction in flow capacity (e.g., Kneller and Branney, 1995). The presence of heterolithic foresets indicates deposition from mud-rich flows (Baas et al., 2016). Millimetric to centimetric mud clasts may travel as bedload, where larger particles skip over a bed of smaller particles (Raudkivi, 1976; García, 2008); however, they might be expected to accumulate preferentially in ripple troughs. Alternatively, they may also be deposited by capacity-driven deposition from a flow containing sand and suspended mudstone clasts. Planar lamination is interpreted to have formed under upper-stage plane-bed conditions (Allen, 1984; Talling et al., 2012). Abrupt changes in basal-bed thickness and onlap terminations onto underlying mudstones are interpreted to result from an interaction with minor seabed topography with downlap representing the pinch-out of beds where flows waned sufficiently to deposit the coarser grained portion of the flow.

Bipartite Bed Facies

Description

Beds consist of a bipartite structure with a lower division comprising weakly normally graded fine-grained sandstone (0.1–1 m thick), with some dewatering structures and rare planar lamination, and occasional mudstone-clast layers (clasts 1–10 cm a-axis). The upper division comprises poorly sorted very fine-grained sandstone and siltstone (0.1–1 m thick) with dispersed sub-angular, elongate, mm-cm scale mudstone clasts and plant fragments (Fig. 3I). Contact between divisions is abrupt and undulating (Fig. 3I).

Interpretation

Bipartite beds form through deposition of the lower division from a sand-rich turbidity current with the "linked" poorly sorted upper division interpreted as deposition from a co-genetic debris flow. Hybrid event beds (Haughton et al., 2003, 2009) are most commonly identified toward the bases and fringes of lobe deposits (e.g., Hodgson, 2009; Talling, 2013). However, they can form in any environment where mud and mudstone clasts are entrained into the turbulent flow, damping turbulence, and developing high-concentration to pseudo-laminar flow conditions (e.g., Ito, 2008; Haughton et al., 2003; Talling et al., 2004; Baas et al., 2011; Pierce et al., 2018).

Thin-Bedded Siltstone and Sandstone

Description

Heterolithic siltstone and sandstone beds (<1–15 cm thick) are normally graded with planar (Fig. 4K), ripple (Fig. 4H), or climbing-ripple laminations. Beds vary in thickness laterally from meters to centimeters over 10s to 100s of meters. Basal beds are sometimes discontinuous, with pinch-out/onlap terminations onto underlying mudstones (Fig. 5). Bioturbation fabric (*Planolites*) is often observed, especially in siltstone dominated packages. Beds can form packages up to several meters thick (Fig. 3J), from siltstone- to sandstone-dominated (Figs. 3J and 3L), and are locally folded and deformed (Fig. 3K).

Interpretation

Normally graded siltstone beds suggest deposition from dilute turbidity currents, with the finer sediment residual within the flow after deposition of the coarser fraction of sediment load (Stow and Bowen, 1980; Jobe et al., 2012). Climbing-ripple lamination forms through late-stage tractional modification by flows, with high-sediment fall-out rates (Lowe, 1988). Low angle of climb suggests higher migration component and lower rates of suspended load fallout and aggradation than in structured sandstone (Allen, 1970; Jobe et al., 2012). Localized deformation and folding indicates slumping of material and/or significant dewatering. Thickness variations, discontinuities and onlap of basal beds are interpreted to result from deposition on irregular seabed topography.

Chaotic Facies

Description

Chaotic beds comprise contorted sand clasts supported by a poorly sorted silt-prone matrix (Fig. 3M). A variant of this facies are poorly sorted, matrix-rich, very fine-grained sandstone to coarse siltstone beds (0.1–2 m thick) that lack internal structure and contain dispersed sub-angular, elongate, mm-cm scale mudstone clasts and plant fragments (Figs. 3M and 4B).

Interpretation

The beds with clasts supported by a poorly sorted matrix are interpreted to have been deposited en masse, and named as debrites (debris-flow deposits; Mulder and Alexander, 2001; Talling et al., 2012).

Folded Facies

Description

Units of contorted and folded strata comprising thin- to thick-bedded sandstones and siltstones can be up to 4 m thick and extend laterally for 10s of meters (Fig. 3N).

Interpretation

These units are interpreted as remobilized deposits formed by slides and slumps.

Regional Mudstone Facies

Description

Claystones and siltstones that have mm-scale laminations are structureless (Fig. 4). This facies forms regionally extensive units that have been mapped for 10s of km (Fig. 3O) and drape every sand-prone unit (Flint et al., 2011; Van der Merwe et al., 2014).

Interpretation

These deposits are interpreted as background hemipelagic deposition.

Environments of Deposition

The thin sandstone Units A/B, B/C, and D/E are interpreted as deep-water lobes due to lateral continuity of beds, lack of major erosion surfaces, and their constituent facies. Four broad environments of deposition have been characterized (Fig. 6) based on the grouping of facies outlined above, mapped geometries, and paleogeographic context, utilizing depositional environment interpretations from previous studies (Prélat et al., 2009; Kane and Hodgson, 2011; Prélat and Hodgson, 2013; Brunt et al., 2013a, 2013b; Morris et al., 2014a, 2014b; Spychala et al., 2015).

Lobe axis: Consisting primarily of thick amalgamated structureless sandstone facies (commonly containing mudstone-clast horizons) interbedded with minor structured sandstone facies (Fig. 6). Lobe axis packages are up to 14 m thick. Typically, contacts with the underlying mudstone are sharp and sometimes scoured with numerous flutes, grooves and other tool marks. In proximal areas of the depocenter, deposits comprise structureless and structured sandstone facies as well as thin-bedded sandstone and siltstone facies. Structured sandstone facies form thin (<5 m) and wide (>100 m) lens shaped packages (Figs. 5E and 6) that onlap, drape, and overtop underlying seabed topography (Fig. 5E). Indicators of sediment bypass include multiple composite scours, with amalgamated erosional surfaces (cm–1.5 m in depth, 0.5–3 m in width) mantled with mudstone-clast lag horizons (e.g., Hofstra et al., 2015; Stevenson et al., 2015).

Lobe off-axis: Consisting of stratified structureless and structured sandstone facies and sand-dominated thin bed facies (Fig. 6). Lobe off-axis packages are up to 5 m thick. Scouring is documented at bed bases and minor erosion is occasionally present throughout. Packages often thicken and thin abruptly with bed thickness changes and onlap of the lower beds onto regional mudstones, due to compensation and infilling of topographic lows.

Lobe fringe: Frontal and lateral lobe-fringe deposits consist of thin structured/structureless sandstone facies with common mud-clast horizons, thin-bedded sandstone and siltstone facies, bipartite beds, and debrites (Fig. 6). Beds are mm to 50 cm thick with lobe fringe packages of thin beds up to 2.5 m and sandstone up to 70 cm. Sand-rich pinch-outs are often associated with clastic injectite networks, up to several meters in thickness and kilometers in lateral extent (Cobain et al., 2017).

Distal lobe fringe: Where fringes are silt-rich, at distal pinch-outs (Fig. 6), deposits consist of thinly bedded siltstone facies with occasional starved ripples. These are distinguished from the regional mudstones as they are coarser than the background sediments and have been walked out from more proximal areas. It may be possible that other packages of distal lobe-fringe facies are present but undocumented.

Hemipelagic drape: This consists of regional mudstone facies and represents periods of clastic starvation in the basin when hemipelagic material can accumulate to regionally extensive, significant (2–10s of meters) thicknesses.

Remobilized packages: These result from syn-sedimentary deformation and can be associated with all environments of deposition, including lobe fringe (Spychala et al., 2017a); levee collapse (Kane and Hodgson, 2011; Morris et al., 2014a); channel margin (Hodgson et al., 2011) and hemipelagic drape (Brunt et al., 2013b). Deposits may represent localized remobilization of packages due to instabilities caused by minor seabed topography (e.g., Spychala et al., 2017a).

Unit A/B, B/C, and D/E Thickness and Facies Distribution

The thin sandstone units are present discontinuously in distinct, spatial areas across the Laingsburg depocenter, with deposition generally concentrated along the western, up-dip Baviaans and Heuningberg locations (Fig. 7). Typically, Units A/B, B/C, and D/E are an order of magnitude thinner than Units A–F (generally <5 m in thickness; Fig. 6), reaching a maximum of 14 m in thickness (Fig. 7). Overall, the thicker areas are dominated by the lobe axis deposits, transitioning to off-axis and fringe deposits laterally and frontally as the unit thins (Figs. 6 and 7).

Unit A/B

In the Baviaans area, flute and groove paleocurrents are consistently toward the north-northeast, changing to eastward around Heuningberg (Fig. 7). Current ripple paleocurrents are more dispersed showing a spread between north-northwest and east. The thickest A/B deposits (up to 14 m) are aligned in a north to south trend, coinciding with the most axial lobe facies (Fig. 6). The unit thins (14 m–1 m) and transitions to off-axis deposits more abruptly (over <3 km) toward Faberskraal and Geelbek to the east and more gradually (over 20 km) to the west, with fringe deposits restricted to the peripheries of the system in Heuningberg, Faberskraal, and Geelbek (Fig. 7). A localized area of increased thickness (up to 10 m) around Heuningberg, thins in all directions (Fig. 7). Lateral pinch-outs (Faberskraal, Geelbek, and Heuningberg) are indi-

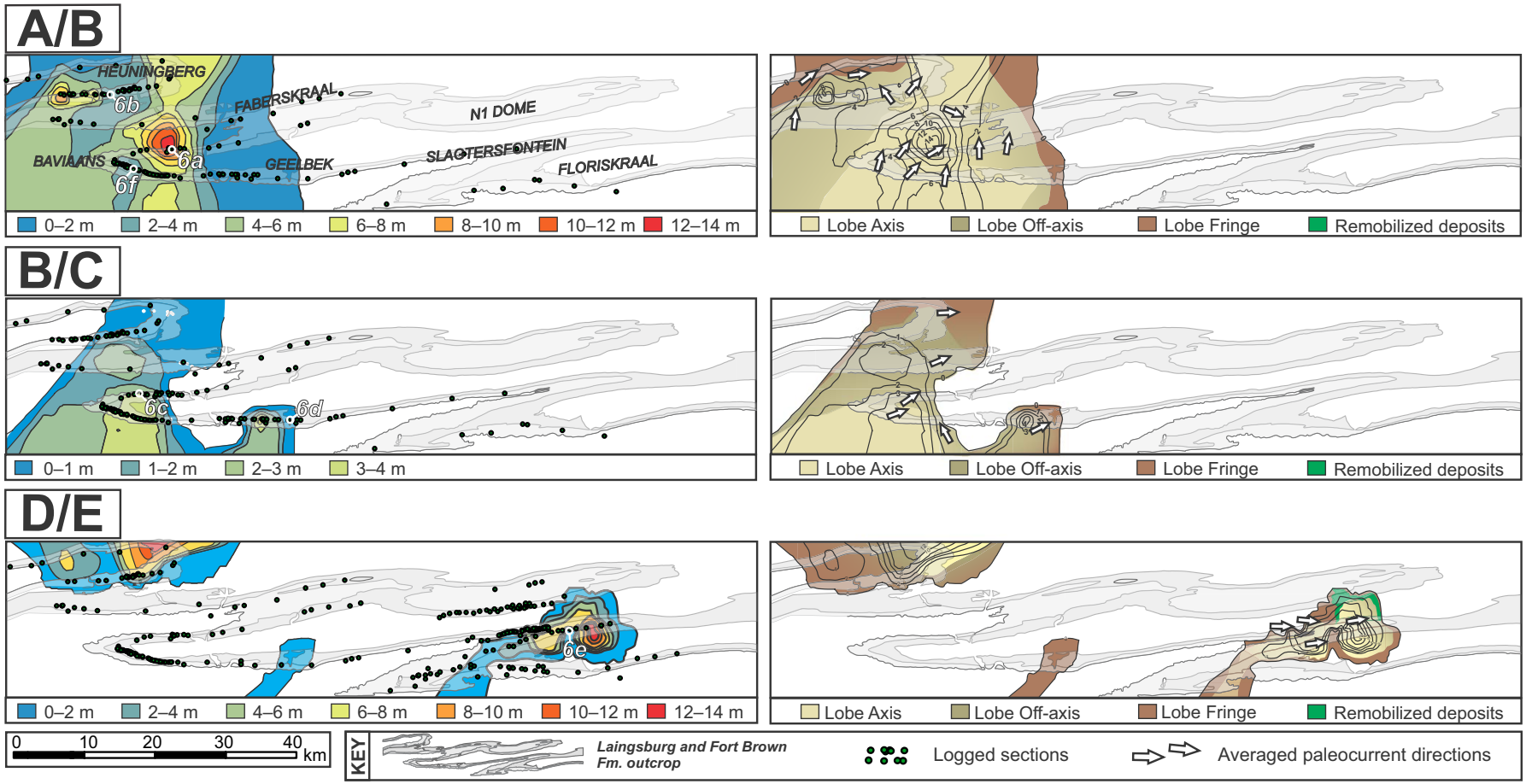

Figure 7. Thickness (left) and facies (right) maps of Units A/B, B/C, and D/E. Thickness maps show isopach contours in meters. Facies maps represent gross depositional environment for the time interval. A/B and B/C deposits are restricted to up-dip of the Faberskraal-Geelbek area. Unit A/B deposits are thickest, most sand-rich and axial in the Baviaans and Heuningberg areas, with bypass dominated proximal lobe scours/distributary channels present in the Baviaans area. Deposits decrease in thickness and sand content to off-axis facies to the east and west. Lobe fringe deposits and pinch-outs are a combination of sand- and silt-rich in Geelbek and Heuningberg. Unit B/C deposits are thickest, most sand-rich and axial in the Baviaans area. Deposits decrease in thickness transitioning from axis to off-axis, and then forming fringe facies gradually to the north and more abruptly to the east and west. Pinch-outs are sand-rich at the lateral east and west margins and silt rich to the north. Unit D/E is present discontinuously in (*a*) Heuningberg, with thick axial deposits abruptly thinning and pinching out west, south and east, (*b*) in Geelbek, present locally as a single debrite bed, and (*c*) in Floriskraal, present in a southeast-northwest transect decreasing in thickness abruptly to the east and west (Slagtersfontein) with sand-rich pinch-out, to the south with a silt rich pinch-out, and more gradually to the north (N1 Dome) with a silt and debrite-rich pinch-out. Logs of sections shown on Figure 6.

cated by a combination of highly discontinuous sand-rich strata and silt-rich thin beds (Figs. 6 and 7). In the most proximal Baviaans area, high aspect ratio erosional features (1–5 m in depth and 10s of meters to 150 m in width) are present over a 10 km strike-oriented outcrop section (Figs. 5E, 6, and 7). Erosional surfaces are overlain by structureless, planar and climbing-ripple laminated sandstone beds that thin and fine laterally to interbedded siltstone and ripple-laminated sandstone (Figs. 5E and 6).

Unit B/C

Unit B/C is also best developed in the regional up-dip areas of the depocenter (Baviaans, Heuningberg, and Geelbek; Fig. 7) with thickest and most axial deposits around Baviaans. Flute, groove, and ripple paleocurrents indicate a northeast direction of transport, with a northwest component at Geelbek (Fig. 7). Unit B/C is thinner overall than A/B (<4 m thick) and less laterally ex-

tensive (Fig. 7). Toward Heuningberg and Faberskraal, deposits transition to off-axis and pinch out more abruptly (Fig. 7). A discontinuous area of thicker (up to 4 m), sand-rich lobe-fringe deposits is present around Geelbek, thinning more abruptly to the west, north, and east, likely related to unexposed axial deposits to the south (Fig. 7). Pinch-outs are sand-rich at the lateral (eastern) fringe (Fig. 6) and more silt-rich and thin-bedded (Fig. 6) toward the frontal (northern) fringe (Fig. 7).

Unit D/E

Unit D/E has been recognized in three discrete sites, correlated though walking key regional markers including top Unit D, base Unit E, and the D-E mudstone. Depositional sites are around Heuningberg, Geelbek, and Floriskraal (Fig. 7). In Heuningberg, up to 14 m of axis and off-axis lobe deposits are present, that thin and transition to fringe deposits to the west, south, and east, pinching out more abruptly to the south and east and more gradually to the west (Fig. 7). In Geelbek, Unit D/E consists of a single debrite bed <2 m thick (Fig. 7). In Floriskraal, a 14-m-thick lobe axis has a southwest to northeast depositional dip oriented pinch-out with paleoflow to the northeast and east (Fig. 7). Unit D/E is highly discontinuous toward Slagtersfontein, transitioning to off-axis and fringe deposits, and pinching out more abruptly to the south and more gradually to the north (Fig. 7). Pinch-outs are more sand-rich (Fig. 6) in the frontal (eastern) fringe and more silt-rich and thin-bedded (Fig. 6) in the lateral (southern) fringe with remobilized/debritic deposits present in the northern lateral fringe (Fig. 7).

Each unit is bounded by a regional mudstone. Locally, below the thin sandstone units silt-rich remobilized strata are present, centimeter to several meters in thickness, ranging from chaotic and highly disaggregated to laterally extensive (meters to 10s of meters).

Interpretation

Facies and thickness distributions indicate A/B and B/C systems were fed from the southwest (Figs. 7 and 8), with mean paleoflow toward the northeast. Lenticular erosive features in the Baviaans area may represent either: shallow scours, often associated with channel-lobe transition zones (e.g., Wynn et al., 2002; Macdonald et al., 2011a, 2011b; Hofstra et al., 2015; Pemberton et al., 2016; Brooks et al., 2018b) formed by hydraulic jumps where flows transition from super- to subcritical due to a reduction in slope gradient and/or flow confinement (Mutti and Normark, 1987, 1991; Weirich, 1989; Kostic and Parker, 2006; Sumner et al., 2013; Dorrell et al., 2016); or weakly confined distributive channels eroding into proximal lobes, with distributive patterns likely due to the reduction of slope gradient (e.g., van der Werff and Johnson, 2003). These characteristics indicate deposition in a base-of-slope area. The distribution of Unit D/E indicates at least two areas of sediment input, in the northeast and to the south (Figs. 7 and 8).

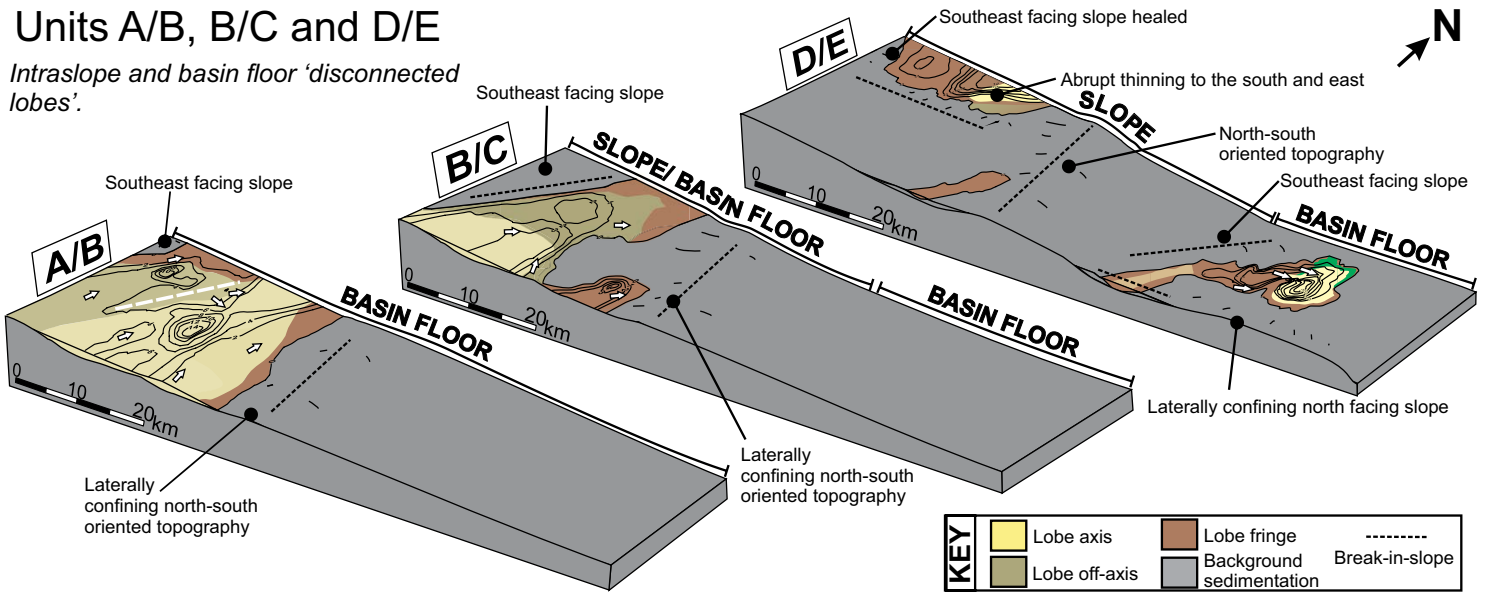

Figure 8. Thickness and facies maps of smaller fan units overlain on 3-D box models demonstrating controlling basin-floor and slope topography.

Similar geographical areas (Faberskraal and Geelbek) of deposition, directions of facies transitions, and thinning and pinch-outs are recognized in all three units (Figs. 7 and 8). Thinning and pinch out of A/B and B/C lobes occur in Heuningberg, where a southeast-facing intrabasinal slope is interpreted to impact flow behavior in the underlying Unit A (Spychala et al., 2017a). We suggest that this intrabasinal slope was present throughout A/B and B/C deposition (Figs. 7 and 8), modifying facies, thickness and paleocurrent trends by reflecting and deflecting flows. The influence of this intrabasinal slope does not persist into Unit D/E deposition indicating that topography was healed by intervening units (Fig. 8).

Eastern pinch-outs in Units A/B, B/C, and of D/E consistently occur across the Faberskraal-Geelbek area (Figs. 7 and 8), suggesting influence by some form of long-lived and relatively fixed, topographic feature (Fig. 8). Lobe pinch-outs indicate a decrease (or slight reversal) in slope gradient, confining deposition up-dip. This topography was apparently fixed in location, but evidently subtle or dynamic, as the effect of large-scale topographic depression is not recognized in the intervening units (Van der Merwe et al., 2014). Therefore, this topography must have formed progressively over time, with a subtle expression on the seabed at any one time (e.g., Spychala et al., 2017a).

The abrupt southward pinch-out of Unit D/E in Heuningberg (Fig. 7) may relate to a north-facing slope, resulting from differential compaction over underlying stratigraphy (Figueiredo et al., 2010). The southwest to northeast–oriented deposition of the Unit D/E axis in Floriskraal (Fig. 8) and pinch-out at Slagtersfontein may be the result of a southeast-facing slope surface representing the regional base-of-slope (Fig. 8). The southward thinning and pinch-out is likely the result of a north-facing lateral basin margin (Fig. 8) (Van der Merwe et al., 2014; Brooks et al., 2018b).

Remobilization within regional mudstones prior to A/B, B/C, and D/E deposition is interpreted to indicate instability of locally steepened frontal and lateral slopes that subsequently controlled lobe deposits and potentially created additional local topography.

DISCUSSION

Units A/B, B/C, and D/E

The dominance of laterally extensive, unconfined, basin-floor lobe deposits within Units A and B (Sixsmith et al., 2004; Prélat and Hodgson, 2013; Van der Merwe et al., 2014) indicates Unit A/B was deposited in a similar basin-floor setting (Fig. 8). Units C, D, and E are interpreted as slope to basin-floor systems (Figueiredo et al., 2010; Van der Merwe et al., 2014; Morris et al., 2014a, 2014b, 2016; Spychala et al., 2015; Brooks et al., 2018b), with the western, up-dip sections on the slope. The co-location of Unit B/C in this area indicates a lower slope setting. Unit D/E in Heuningberg and Geelbek likely represents intraslope lobes (Spychala et al., 2015), with the Floriskraal deposits on the basin floor (Fig. 8).

Unit A/B, B/C, and D/E lobe deposits are subdivided into axis, off-axis and lateral/frontal fringe (Fig. 6), with similar facies transitions in lobes and lobe complexes (sensu Prélat et al., 2009) recognized in the larger units. These units rarely record juxtaposition of multiple sub-environments (Fig. 6), indicating that deposition was not sufficiently sustained or sediment volume was not adequate for lobes to stack. Neither compensational stacking to form a lobe complex, nor propagation of channel-levee systems above lobes (e.g., Morris et al., 2014b; Hodgson et al., 2016) is documented in these units. In addition to thickness, A/B, B/C, and D/E show key differences in facies and architecture to the larger Units A–F (cf. Sixsmith et al., 2004; Prélat et al., 2009, 2010; Prélat and Hodgson, 2013). These include (a) a higher proportion of sand (Figs. 4 and 6) particularly in frontal fringes (Fig. 6); (b) consistently sharp bases and tops (Figs. 4 and 6); (c) a higher proportion of mudstone clasts (Figs. 4 and 6); (d) minor (<1 m) basal scouring throughout, including at fringes (Figs. 5 and 6); (e) significant and widespread abrupt thinning and pinch out causing discontinuity (Figs. 5 and 7), rarely associated with facies changes; and (f) weakly confined channels/scours in proximal area of lobes. Similar to the larger units, lateral fringes are recognized as more silt-rich and thin-bedded whereas frontal fringes are sand-rich and discontinuous (Fig. 6). This variation is also documented in the Tanqua depocenter (Rozman, 2000; Prélat et al., 2009; Groenenberg et al., 2010) and is interpreted to relate to differences in flow processes in distal frontal versus distal lateral run outs (Spychala et al., 2017b).

Units A/B, B/C, and D/E stratigraphically overlie the thickest regional mudstone units in the Laingsburg and Fort Brown formations (Grecula et al., 2003; Di Celma et al., 2011; Van der Merwe et al., 2014), and are interpreted as the deposits from the first flows after the longest period of clastic shut off in the deep water part of the basin, reflecting the longest duration relative sea-level rise (Flint et al., 2011). Flint et al. (2011) suggested these units were distal expressions of larger scale lobe complexes similar to Units C–F. However, key differences in sedimentology and architecture described above indicate this is not the case. The absence of persistent supply that may drive lobe stacking and propagation of channel-levee systems (Fig. 8) suggests the thin units may not have been fully connected to upper slope and shelf feeder systems (Fig. 9). Delta propagation to the shelf edge, or across-shelf sediment bypass, may have been insufficient to activate upper slope (e.g., canyon) systems and sediment may have been sourced directly from the outer shelf region and via slope failures (Fig. 9). A range of input directions may have resulted in weakly confined flows, unrestricted to long-lived conduits (e.g., Saller et al., 2004; Moody et al., 2012; Stevenson et al., 2013). Multiple, short-lived sediment input locations would create widespread areas of lobe deposition. The interaction of deposits produced by these multiple inputs, would lead to lobes that do not stack compensationally or aggradationally (Fig. 9). A lack of significant channelization could cause flows to traverse completely “out-of-grade” areas (sensu Prather, 2003) that would erode the slope, driving entrainment of mud clasts. Unconfined flows would spread laterally (Al Ja’Aidi et al., 2004; Kane et al., 2008; Hamilton et al., 2017) and be more susceptible to topographic perturbations than more channelized flows (Kneller and Buckee, 2000).

Formation of larger fan units

- Relative sea-level fall exposes shelf break/ brings delta to shelf edge.
- Canyon systems are active.
- Additional sediment supply from shelf sands and slope failures.
- Flows are confined creating consistent flow pathways.
- Clearly defined channel systems develop.
- Channels propagate over lobes.
- Compensational and aggradational lobe stacking depending on seabed topography.

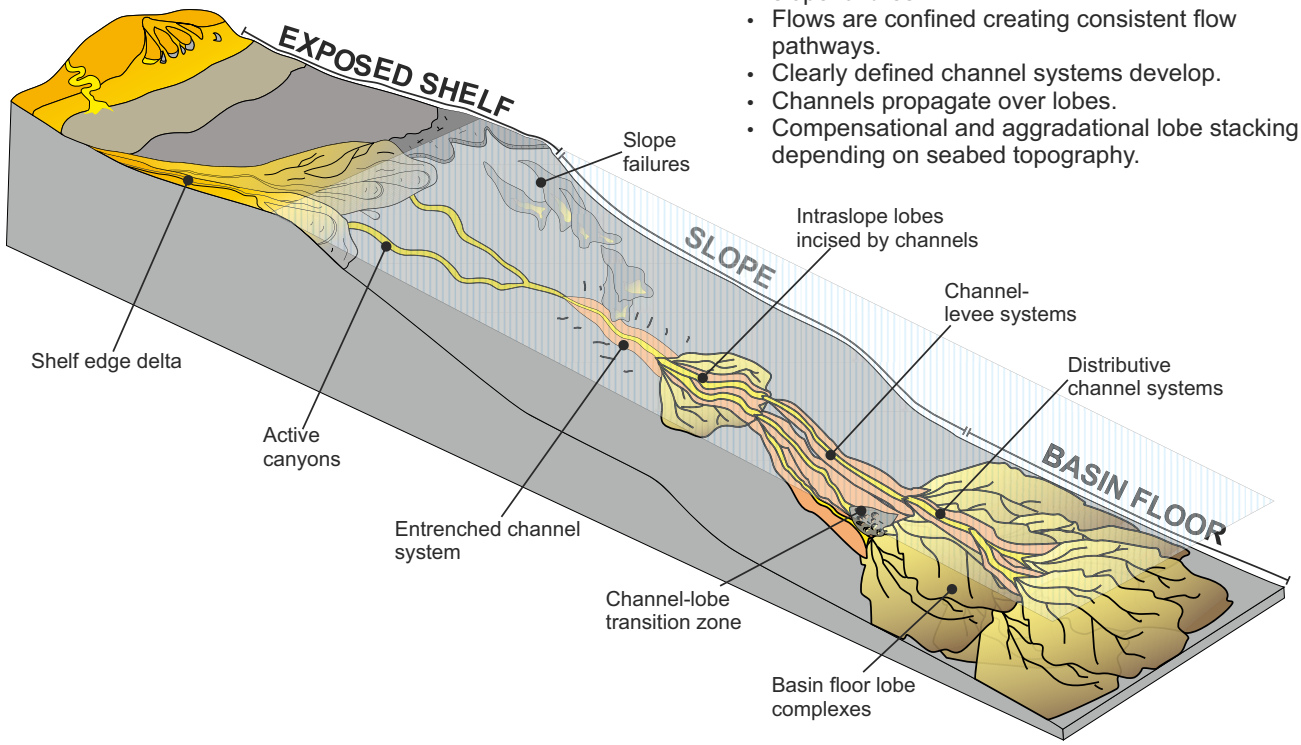

Formation of 'disconnected lobes'

- Relative sea-level fall insufficient to expose shelf break/ bring delta to shelf edge.
- Canyon systems inactive/ less active.
- Sediment supply from shelf sands and slope failures.
- Flows are unconfined to weakly confined creating inconsistent flow pathways.
- No clearly defined channel systems.
- No propagation of channels over lobes.
- Insufficient sediment supply for lobe stacking.

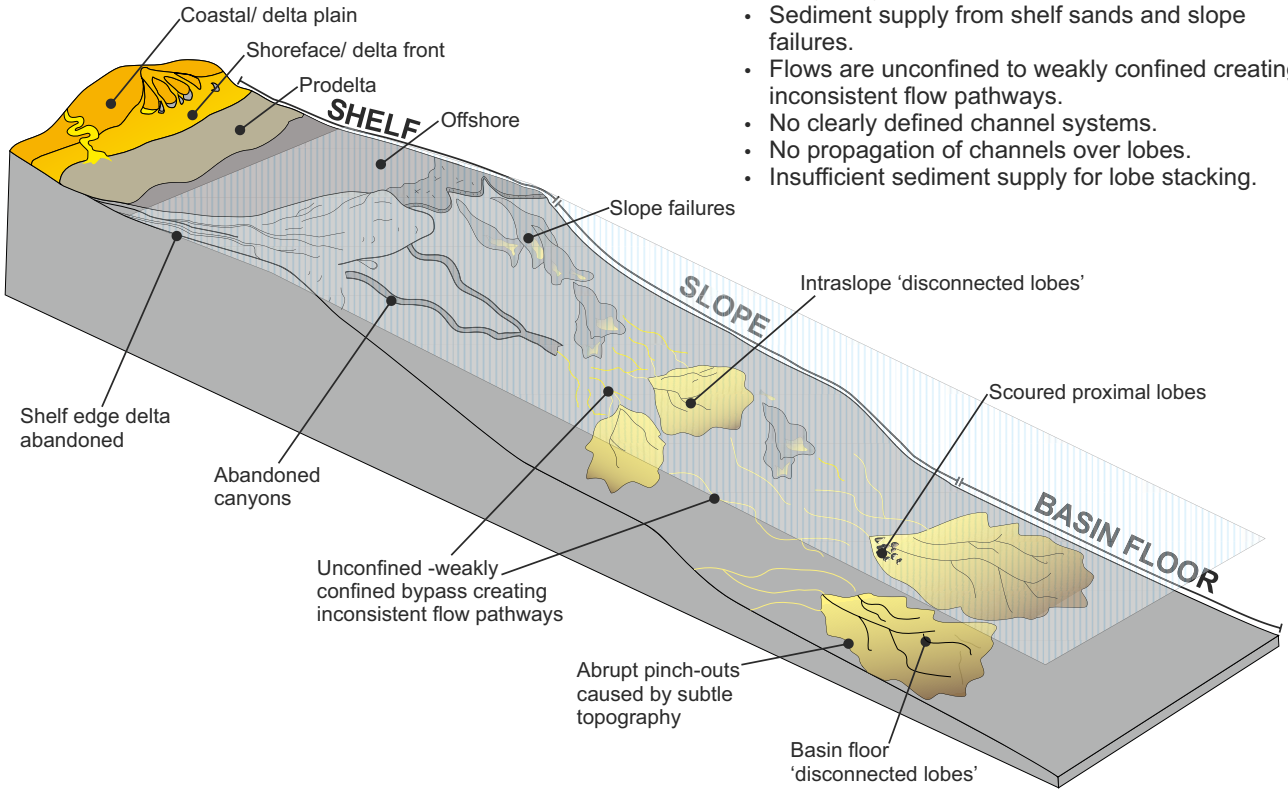

Figure 9. Shelf, slope, and basin-floor profile during deposition of larger fan units and "disconnected lobe" forming smaller fan unit. Lower sea level during deposition of larger units exposes the shelf and/or brings deltas to the shelf edge and activates canyons on the upper slope connecting sediment pathways down the slope. Comparatively greater relative sea level fall during deposition of smaller units reduces and/or cuts off main sediment input.

Disconnected upper slope feeder systems would suggest that relative sea-level falls were not of sufficient magnitude or duration to expose the shelf or bring the deltas close to the shelf edge (Fig. 9). Therefore, small-scale rises in relative sea level (or autogenic adjustment of the shelf delta or slope equilibrium) would be sufficient to cut off sediment supply to the deep water. Initiation of Units A–F is interpreted as marking times when relative sea-level fall was sufficient to expose the shelf and/or bring the delivery systems to the shelf edge and activate upper slope feeder systems (Fig. 9). The lobe deposits of Units A/B, B/C, and D/E are therefore interpreted as "disconnected lobes" that are characterized by supply from short-lived conduits, such as slope gullies or locally developed incipient channels, rather than point-sourced flows through mature channel-levee systems (Fig. 9). It is also possible that other methods of long-term (i.e., 100,000s to millions of years' time scale) allogenic forcing could have influenced shelf and slope sediment delivery systems resulting in the variation of sediment input.

These disconnected lobes can be compared to models of intraslope lobes (also known as perched lobes; Plink-Björklund and Steel [2002]; Prather et al. [2012a]; or transient fans; Adeogba et al. [2005]; Gamberi and Rovere [2011]). These models based on shallow seismic reflection data sets have been interpreted to show initial stages of fully confined ponded facies, transitioning stratigraphically through partially confined wedge shaped fill, and finally bypass stages (Prather et al., 1998; Prather, 2000). In contrast, the disconnected lobes herein show no evidence for initial ponding, although onlap and downlap is documented. The absence of graded bed tops throughout the units and lack of fines suggest downstream flow-stripping (Sinclair and Tomasso, 2002; Spychala et al., 2015) occurred, and that the upper, finer portions of the flow were able to surmount the topographic confinement and bypass down-dip. This indicates slope topography was not of sufficient magnitude or three-dimensional constraint to completely pond flows (e.g., Haughton, 1994). Moreover, although units have a sharp top, late-stage sediment bypass is also not documented in these disconnected lobes suggesting slope accommodation remained underfilled.

Slope to Basin-Floor Topography through Units C, D, E, and F Deposition

The depositional trends documented in Units A/B, B/C, and D/E indicate subtle seabed topography was maintained over relatively long periods, resulting in a persistent location of pinch-out. Here, we discuss topographic indicators present in the thicker, more laterally extensive Units C, D, E, and F (Figs. 10, 11, 12, and 13A), that have been mapped in detail in previous studies (Grecula et al., 2003; Figueiredo et al., 2010; Di Celma et al., 2011; Hodgson et al., 2011; Brunt et al., 2013a; Van der Merwe et al., 2014; Spychala et al., 2015; Morris et al., 2016; Brooks et al., 2018b).

Intraslope Lobes

Intraslope lobe complexes have been recognized in subunits E1, E2, and E3 with maximum thickness of 5, 15, and 20 m, respectively, and within subunits F1 and F3 with maximum thicknesses of 5 and 35 m, respectively (Fig. 11) (Figueiredo et al., 2010; Van der Merwe et al., 2014; Spychala et al., 2015). All intraslope lobe complexes have an eastern down-dip pinch-out in the Faberskraal-Geelbek area (Figs. 11 and 13A), marking the presence of a persistent area of local accommodation (Fig. 11) (Figueiredo et al., 2010; Van der Merwe et al., 2014; Spychala et al., 2015). At any one time, the amount of accommodation would have been subtle, but long-term development in fixed locations led to a marked impact on the stratigraphic architecture of the basin fill (Figs. 12 and 13A).

Unlike the smaller fan units, these intraslope lobe complexes (Units E and F) demonstrate a stratigraphic transition through initial deposition and infill of slope accommodation by lobe deposits (E2 and F2; Figure 11) and later stage sediment bypass through channel-levee systems (E3 and F3; Figure 11), similar to that documented in the Niger Delta slope (Prather et al., 2012a; Jobe et al., 2017; Fig. 1E) and various basins throughout the Gulf of Mexico (Prather et al., 1998, 2017; Fig. 1D). This indicates that sediment input was sufficient for slope accommodation to become healed.

Slope Channel Systems

The long-lived feeder system present around Baviaans throughout Units C and D time has been well documented (Fig. 10) (Hodgson et al., 2011; Kane and Hodgson, 2011; Brunt et al., 2013a; Morris et al., 2014a, 2016). This system varied from entrenched up-dip to more distributive down-dip, and has been documented within subunits C2, D1, D2, and D3 across the Faberskraal-Geelbek area (Fig. 10) (Brunt et al., 2013a; Van der Merwe et al., 2014; Morris et al., 2014a, 2016). Due to the spatial coincidence with intraslope lobe complex pinch-outs (Figs. 10 and 13A), it is possible that a reduction in slope gradient caused flows to decelerate, decreasing their ability to erode.

Sediment Bypass–Dominated Zones

Zones of coarse sediment bypass (sensu Stevenson et al., 2015) have been recognized within Units E and F (Van der Merwe et al., 2014; Brooks et al., 2018b), within the central area of the depocenter, between Faberskraal/Geelbek and N1 Dome/Slagtersfontein (Figs. 11 and 12), indicating a persistent area of decreased accommodation, on a slope close to equilibrium (Prather, 2003). The zone is characterized by thin channel-levee deposits and the formation of sediment bypass-dominated channel-lobe transition zones (CLTZs) (e.g. Mutti 1985; Mutti and Normark, 1987, 1991; Wynn et al.,

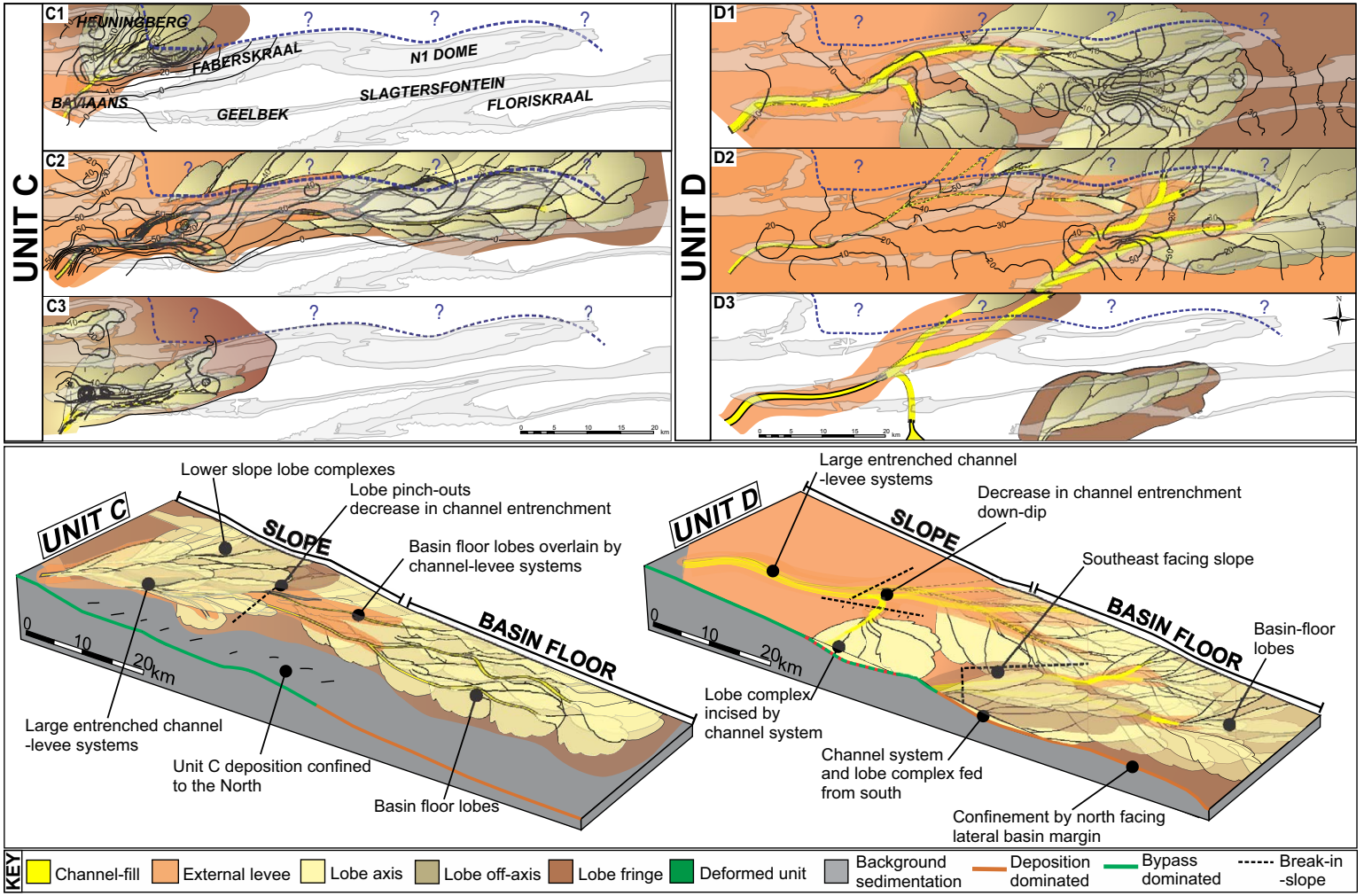

Figure 10. Thickness and facies maps of Units C and D. Thickness is shown as isopachs with units in meters. Facies maps represent gross depositional environments for the given time intervals. Based on studies by Sixsmith et al. (2004); Di Celma et al. (2011); Hodgson et al. (2011); Brunt et al. (2013a); Morris et al. (2014a, 2016); Van der Merwe et al. (2014). Thickness and facies maps of "sand-attached" Units C and D overlain on 3-D box models demonstrating controlling slope to basin-floor topography.

2002) at Slagtersfontein within Unit E (Brooks et al., 2018b) and the N1 Dome within Unit F (Figs. 11 and 12). These CLTZs represent the regional base-of-slope indicated by paleogeographic context and facies transitions from channel-levee systems to unconfined basin-floor lobe complexes (Brooks et al., 2018b; Fig. 11). This slope is interpreted as southeast facing during Unit E deposition, due to the orientation of up-dip lobe pinch-outs (Fig. 11). Zones of coarse-sediment bypass in Units E and F likely indicate an increase in slope gradient in this central area in order for flows to bypass efficiently and the development of the step-ramp-step geometry (Brooks et al., 2018b; Fig. 11). Absence of Units D/E and subunit D3, as well as the thinning of subunit D2 in the central area, may be early indicators of this ramp slope (Figs. 7, 10, and 12).

Basin Floor

Within subunits E2 and E3, tabular, laterally continuous (kilometers in dip and strike), thin bedded siltstone packages (spill-over fringe deposits) are recorded beneath the basin-floor lobes (Brooks et al., 2018b; Fig. 11), and reflect

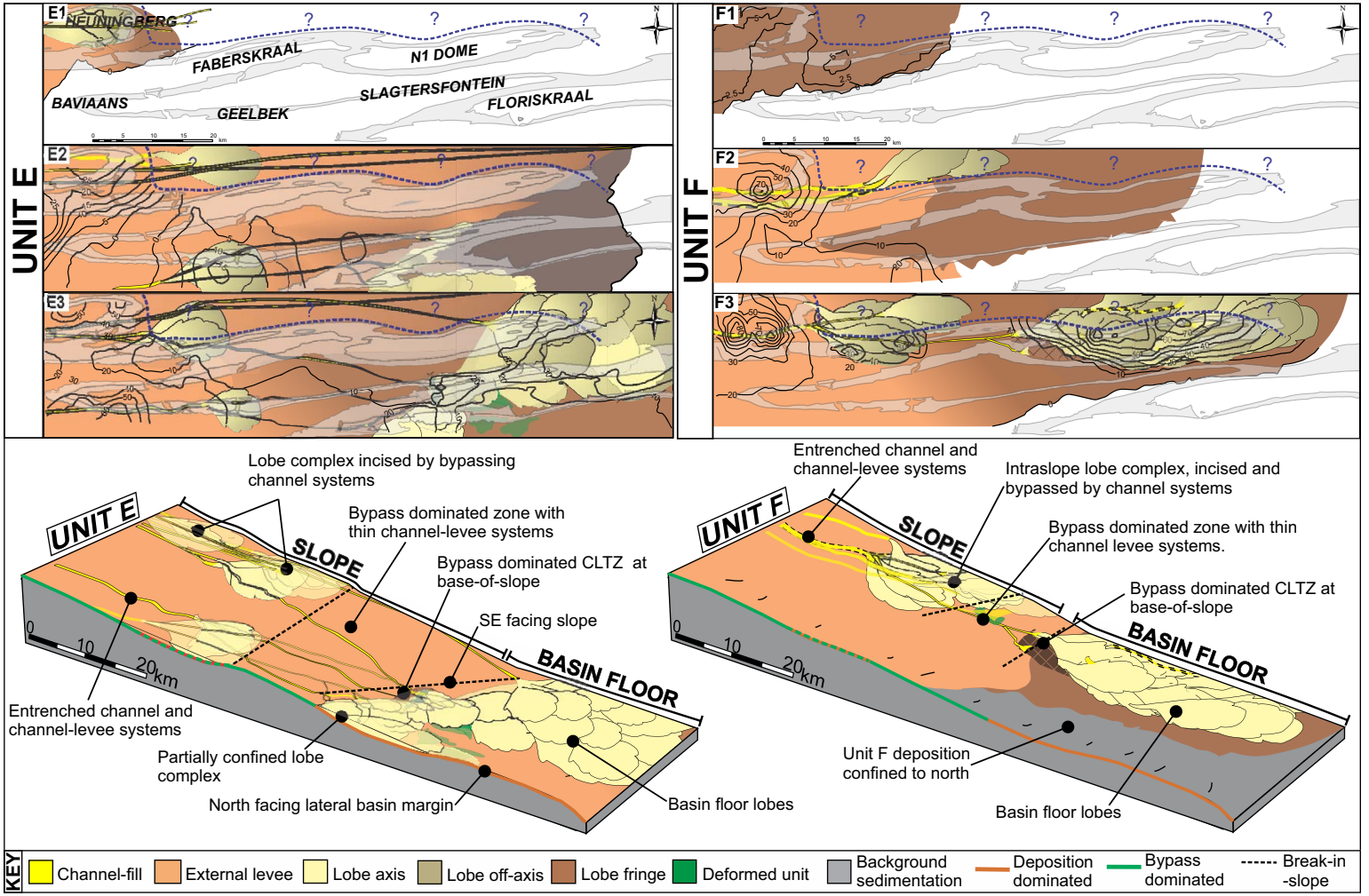

Figure 11. Thickness and facies maps of Units E and F. Thickness is shown as isopachs with units in meters. Facies maps represent gross depositional environments for the given time intervals. Thickness and facies maps of "sand-detached" Units E and F overlain on 3-D box models demonstrating controlling slope to basin-floor topography. Based on studies by Figueiredo et al. (2010, 2013); Van der Merwe et al. (2014); Spychala et al. (2015); and Brooks et al. (2018b). CLTZ—channel-lobe transition zone.

initial flow stripping of fines and trapping of sand in intraslope lobes (Sinclair and Tomasso, 2002). Later channels incised into the intraslope lobes (Fig. 11) (Spychala et al., 2015), indicating that accommodation was filled and the slope was at grade.

Early Basin-Floor Topography Development and Evolution

In order to understand when the fixed seabed topography initiated, a 3-D datacube was constructed in Petrel® using the laterally persistent Whitehill Formation as a basal datum and regional mudstones to correlate units throughout the entire Laingsburg depocenter. Figure 13B shows a dip section of the Vischkuil, Laingsburg, and Fort Brown formations, highlighting two distinct areas of increased thickness separated by a zone of thinning in all units. Thickness maps have also been constructed using this datacube, from the early stage starved basin plain deposits and mass-transport deposits of the Collingham and Vischkuil formations through the overlying basin-floor lobes of Units A and B in the Laingsburg Formation (Fig. 13B). The Collingham, Vischkuil, and Laingsburg formations (Fig. 13B) have the same general thickness patterns as the overlying units, with thicker deposits in the west, thinning in the central area and thickening to the east and southeast.

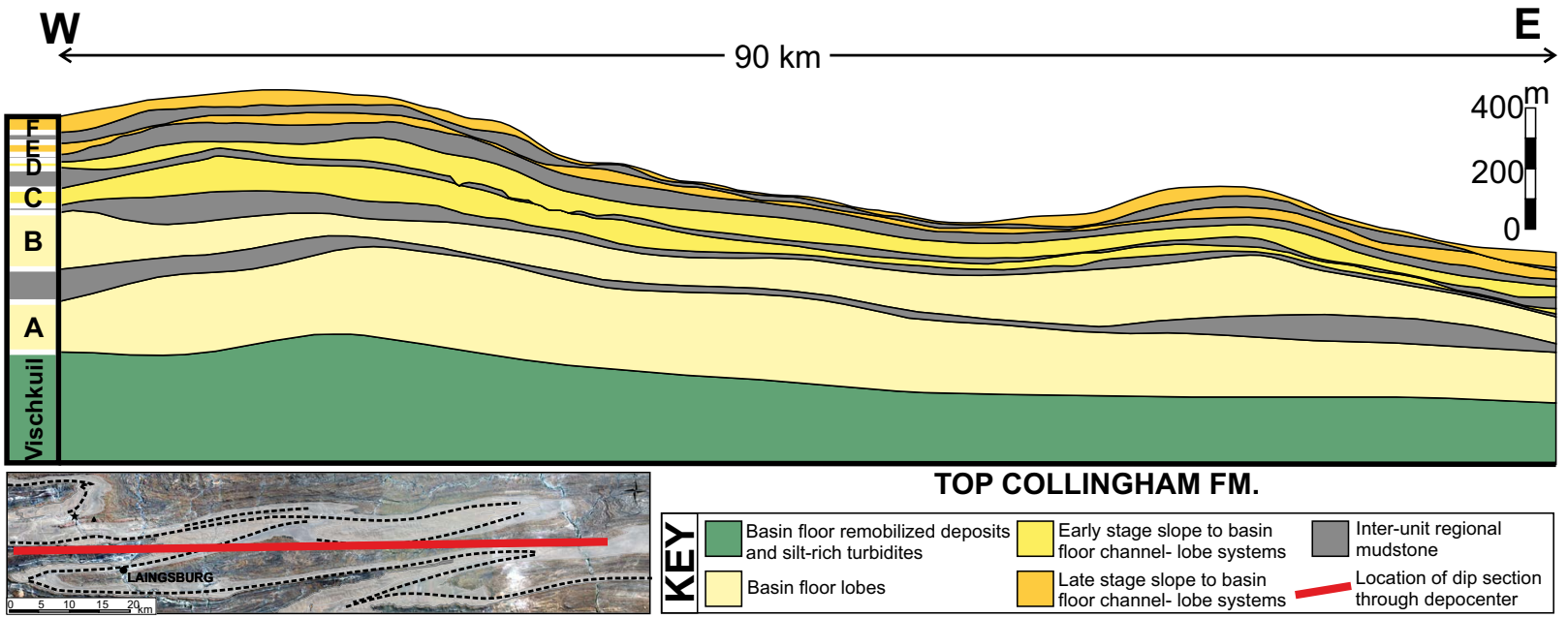

Figure 12. Dip-section through central line of Laingsburg depocenter showing thickness of Vischkuil, Laingsburg and Fort Brown formations. The section demonstrates system scale compensational stacking between units as well as the prevalence of two separate areas of increased deposition with an intervening area of thinning, exacerbated by differential compaction.

The repeated thickness and facies trends across all units (Figs. 12 and 13) indicate the presence of fixed locations of persistent topographic influence and suggest that the systems were not "at grade" (sensu Prather, 2003) at the initiation of deposition. An "out of grade" slope was generated during deposition of the thick regional mudstones of the transgressive and highstand sequence sets within each composite sequence. The rate of accommodation creation was outpaced by sedimentation during deposition of lowstand clastic units. Therefore, longer hiatuses in sand input, inferred from higher mudstone thicknesses (see Figs. 12 and 14), would lead to higher amplitude intraslope accommodation, with Units A/B, B/C, and D/E deposited during these times.

The thinning of the Vischkuil Formation as well as Units A and B (Fig. 13B), the absence of A/B, B/C, and D/E (Fig. 7), the thinning of Units C and D (Fig. 10), and the formation of sediment bypass dominated zones in Units E and F (Fig. 11) all occur in the central area (Figs. 12 and 13). This indicates a long-lived area of reduced accommodation, interpreted as a long-lived higher gradient "ramp" within a stepped slope profile (e.g., Figs. 1B and 1C). This stepped profile had a more acute impact in the later Units E and F (Figs. 11 and 12) (Van der Merwe et al., 2014; Brooks et al., 2018b), but was present to some extent from the onset of deep-water sand supply to the depocenter (Fig. 13B).

The cause of the protracted deformation of the slope is unknown, but it is clear that it was active prior to the onset of sand deposition (Unit A) in the basin (Fig. 13B). Influence of inherited seabed topography alone (e.g., Adeogba et al., 2005; Gamberi and Rovere, 2011; Olafiranye et al., 2013) cannot be the reason as it would be healed over time. Dynamic mechanisms such as salt diapirism and mobile shale (e.g., Barton, 2012; Deptuck et al., 2012; Hay, 2012; Prather et al., 2012a, 2012b), have the potential to create significant and reoccurring accommodation such as in the Gulf of Mexico (Prather et al., 1998; Prather, 2000; Meckel et al., 2002), but are not present in the stratigraphy. Active tectonic structures can also create topographically complex slopes (e.g., Hodgson and Haughton, 2004; Burgreen and Graham, 2014). However, no large-scale syn-sedimentary tectonic structures are documented in the Karoo Basin, although it is possible that structures could be present at high angles to the post-depositional fold structures associated with the deformation front of the Cape Fold Belt. The characterization of the Karoo Basin as a thermal sag basin related to subduction dynamic topography (Tankard et al., 2009) suggests that differential subsidence or localized uplift could be possible mechanisms for generating this deformation. The repeated accommodation created west of the Faberskraal-Geelbek area indicates this area was undergoing subsidence at an increased rate compared to east of the area. This could indicate increased

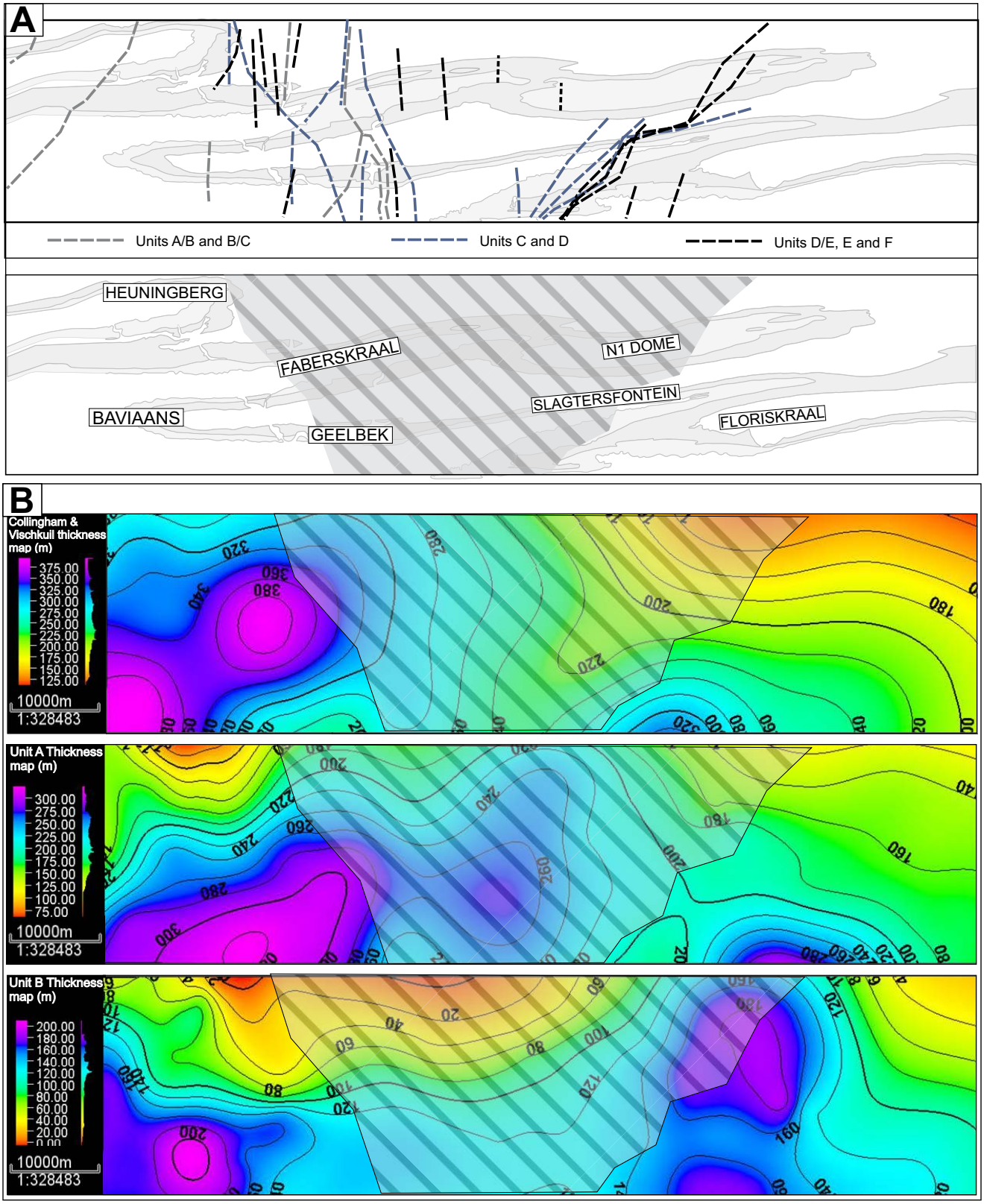

Figure 13. (A) Lobe up-dip, down-dip, and lateral pinch-outs of smaller and larger units color coded into stratigraphic packages. Gray-striped shaded area indicates the region of sustained topographic influence throughout deposition of all units. (B) Thickness maps of the combined Collingham and Vischkuil formations, Unit A and Unit B. Overlay shows area of sustained topographic influence.

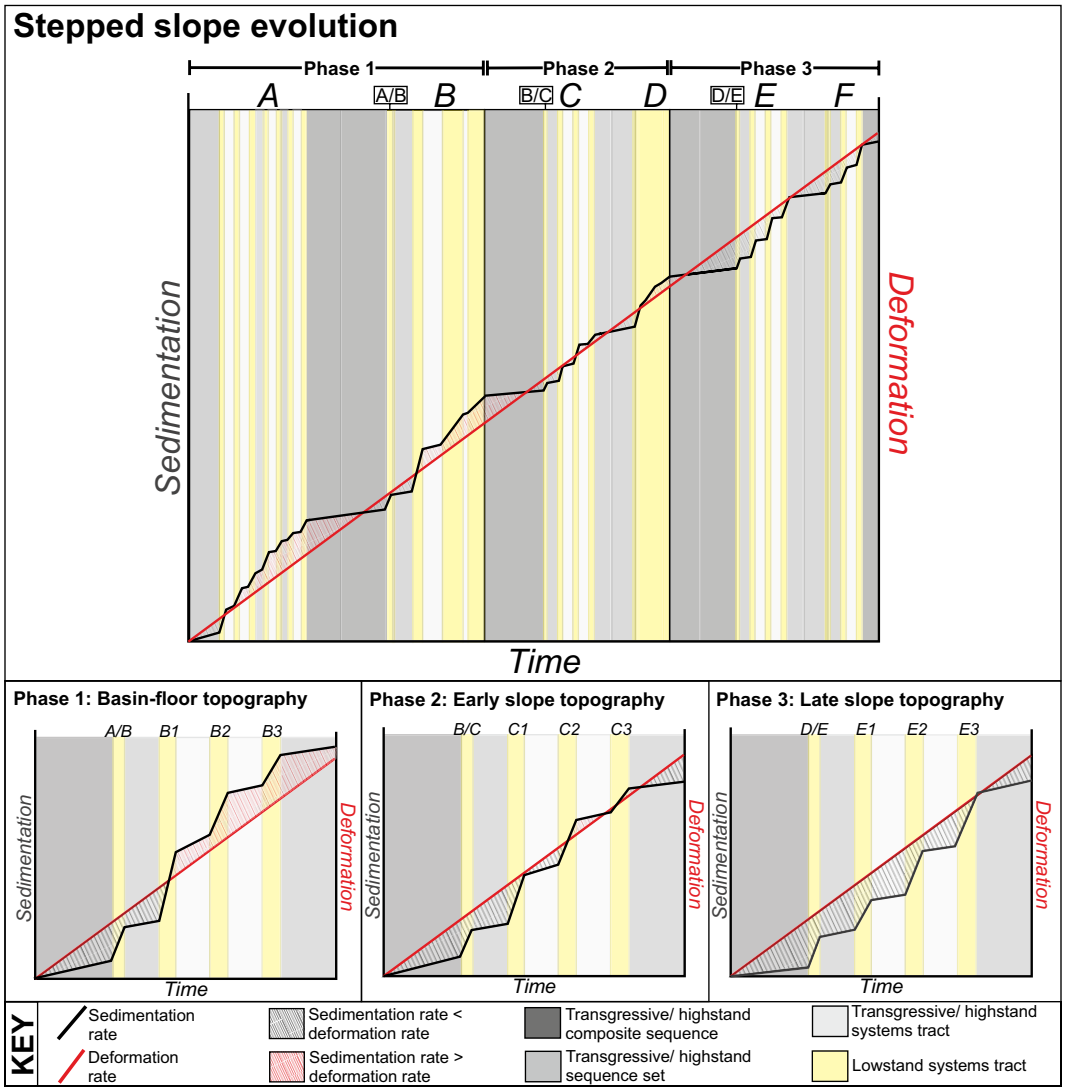

Figure 14. Graph showing comparison of sedimentation and deformation rates throughout the deposition of the Laingsburg and Fort Brown formations. Phase 1 includes Units A, A/B, and B; overall sedimentation rate outpaces deformation rate, with Units A/B deposited onto a comparatively more deformed slope. Phase 2 includes Units B/C, C, and D; overall sedimentation rate was roughly equal to deformation rate, periodically healing and overspilling slope topography in times of increased sedimentation. Phase 3 includes Units D/E, E, and F; overall deformation rate outpaced sedimentation rate. Sedimentation rate was only sufficiently high during the later stage subunits E3 and F3 to equal deformation rate.

subsidence relative to the overall subsiding basin, or a stationary/uplifting basement block east of Faberskraal-Heuningberg, resulting in a steeper slope, leading to the formation of the E and F sediment bypass dominated zones. Thermal subsidence can vary with upper crustal heterogeneity or thickness of basement, which are variable across the Karoo Basin (Binks and Fairhead, 1992; Bumby and Guiraud, 2005) or with spatial variations in mantle downwelling and crustal heterogeneity (Tankard et al., 2009), with magnetic anomalies in the underlying basement (Weckmann et al., 2007; Tankard et al., 2009; Lindeque et al., 2011) indicating the existence of a highly complex upper crust.

Phases of Slope Evolution

Overall, three key stages of stepped slope evolution are interpreted in the Laingsburg depocenter (Fig. 14). In the absence of a strong chronostratigraphic

framework, the rate of slope deformation is assumed to be constant, with variations in sediment input and the stacking of systems resulting in varying stages of topographic influence.

- Phase 1 (Fig. 14; Units A, A/B, and B). These units were deposited at a time of high sediment supply, outpacing deformation rate, healing accommodation created during times of sand shut off (Fig. 14). During early stages of Unit A sedimentation, healed slope accommodation (sensu Prather, 2000, 2003) dominated. Due to the longer term sand shut off between the Unit A and B composite sequence sets, it is likely Unit A/B and initial Unit B flows were deposited in partially confined healed slope accommodation. During Unit A and B deposition, sedimentation rate was sufficient to outpace the deformation rate, allowing depositional and erosional patterns to modify the basin-floor profile toward equilibrium.
- Phase 2 (Fig. 14; Units B/C, C, and D). These units were deposited at a time of moderate sediment supply, in balance with deformation rate, with phases of healing and degradation of the slope (Fig. 14). The shut-off of sand supply during the B-B/C transgressive and highstand sequence set caused B/C to commence deposition on a deformed slope (Fig. 14). Therefore, Unit B/C and initial Unit C sedimentation likely occurred above partially confined slope accommodation with continued C and D deposition filling and healing slope accommodation (sensu Prather, 2003). The entrenched channel systems (Fig. 10) show that slope profile was above grade and undergoing erosion to establish a graded profile (e.g., Pirmez et al., 2000; Deptuck et al., 2012; Hay, 2012).
- Phase 3 (Fig. 14; Units D/E, E, and F). These units were deposited at a time of lower sediment supply, with deposition commencing on a more deformed slope after the D-D/E transgressive and highstand sequence set sand shut-off. Units D/E, E1, F1, and F2 were deposited in intraslope accommodation, with E2, E3, and F3 deposited in healed slope accommodation (sensu Prather, 2003) where they evolved to "fill and overspill" accommodation to bypass sediment down-dip (e.g., Prather et al., 1998; Beaubouef and Friedmann, 2000; Pirmez et al., 2000; Booth et al., 2003; Barton, 2012; Bohn et al., 2012).

Overall, this evolution demonstrates the transition from a relatively "simple" slope to basin-floor profile (Fig. 1A) to a stepped slope profile (Figs. 1B and 1C) with development of healed, but not ponded accommodation (sensu Prather, 2003). Previous studies have demonstrated that stepped slopes evolve temporally, often attributed to active mobile substrates or tectonics (Prather, 2003; Hay, 2012; Jobe et al., 2017; Fig. 1E), healing of mini-basins (Satterfield and Behrens, 1990; Prather et al., 1998; Prather, 2003), or through healing of initial mass-wasting generated slope relief (Shultz and Hubbard, 2005; Romans et al., 2011; Brooks et al., 2018a). An example of topographic relief being healed through time (Phase 1, Fig. 14) is the Tres Pasos Formation, Chile, where initial mass wasting resulted in an out of grade slope profile (Shultz and Hubbard, 2005; Armitage et al., 2009) that was subsequently smoothed to permit progradation of the slope (Hubbard et al. 2010; Romans et al., 2011). However, exhumed submarine slope systems with the required stratigraphic control and spatial extent to document increasing topography of submarine slope systems are rare and tend to come from small tectonically active basins with steep slopes (e.g., Haughton, 1994; Haughton, 2000; Hodgson and Haughton, 2004; Kane et al., 2010; Moody et al., 2012). Therefore, this study of the impact on stratigraphic architecture during long-term evolution of subtle slope topography over a large area is unique.

This study demonstrates that stepped slope profiles (e.g., Figs. 1B and 1C) can evolve from relatively "simple" slope profiles (e.g., Fig. 1A) without mobile substrate (e.g., Figs. 1D and 1E), significant tectonic deformation or mass wasting, instead forming through subtle slope deformation, stacking of multiple systems and significant periods of coarse clastic shut off, allowing deformation to outpace depositional healing (Fig. 14). This highlights a key consideration suggested by previous seismic reflection studies (e.g., Prather, 2003; Jackson et al., 2008) that the size and scale of deformation compared to sedimentation rate is critical, and that systems with episodic sediment flux form more slope accommodation than those without (Prather, 2000, 2003). We have shown that subtle, but slow, and persistent deformation over a significant area of a slope (many kilometers) with significant periods of sand shut off (e.g., between Units D and E deposition) can modify sediment delivery pathways and consequently sand distribution to an extent comparable to that generated by more obvious mobile substrate and tectonics. This has implications for hydrocarbon reservoir prediction within slope systems (e.g., Western Niger Delta, Deptuck et al., 2012; Gulf of Mexico, Prather et al., 1998, Prather, 2000, Meckel et al., 2002; and Offshore Angola, Hay, 2012) which have become increasingly significant as exploration targets in many basins worldwide (e.g., Weimer and Link, 1991; Mayall et al., 2006).

CONCLUSIONS

Thickness and facies distributions of Units A/B, B/C, and D/E, including persistent areas with the presence or absence of sand deposition, indicate a strong influence of fixed seabed topography on the slope and basin floor. These units vary from the larger units in the Laingsburg and Fort Brown formations, due to their thin, sand-rich nature, with evidence of increased erosion, and lack of lobe stacking or channel propagation. These thin units are interpreted to represent the first sand supply to the deep basin following extended periods of high sea levels. Characteristics of the thin units are interpreted as marking only partial re-establishment of sand delivery pathways, here termed "disconnected lobes," which are not sourced from major feeder channel-levee systems, but from periodic failures on the shelf edge and upper slope. Such disconnected lobes vary from intraslope lobes in the Laingsburg depocenter and other systems, due to their stratigraphic position and limited deposit thickness, as a result of their formation within the initial stages of long-term relative sea-level fall. In contrast, larger Units A–F likely formed in periods of lower sea level that were sufficient to bring delivery systems to, or close to the shelf edge, developing and reusing mature upper slope sediment distribution pathways.

Persistent areas of increased or decreased thickness in the underlying formations suggest that the topography was developed before onset of major sand input to the basin. Overall, three stages of evolution are recognized, with a temporally increasing impact on slope to basin-floor systems. In Phase 1, sedimentation rate outpaced deformation rate. During Phase 2, sedimentation rate was roughly equal to deformation rate. Finally, in Phase 3, sedimentation rate was outpaced by deformation rate, with the stepped slope topography showing a dominant control on depositional architecture. The cause of deformation is unknown but may relate to differential subsidence across basement heterogeneities. The model presented here can be applied to identify accommodation change and deep-water system architecture across evolving stepped slope profiles. This study indicates that subtle but persistent deformation, paired with significant periods of clastic shut off, can have a comparable impact to mobile substrate, active tectonics, or mass wasting on sediment routing.

Flows sourcing the thinner discontinuous sand units tend to deposit in topographic lows and deflect around highs, consequently persistent areas of presence/absence can indicate long term topographic influence, making these units more reliable topographic indicators than larger units which often modify the slope profile as they deposit.

ACKNOWLEDGMENTS

The authors thank the local farmers of the Laingsburg area for permission to undertake field studies on their land. De Ville Wickens helped with regional context and logistical support. We thank Rachel Harding for the construction of datacube figures. We thank Sarah Cobain, Florian Pohl, Lewis Burden, Sophie Cullis, and Grace Cosgrove for field assistance. This work was carried out as part of the SLOPE 4 consortium research project. We are grateful for financial support from: Anadarko, BHP Billiton, BP, ConocoPhillips, ENGIE, Maersk Oil, Murphy, Nexen, Petrobras, Premier Oil, Shell, Statoil, Total, VNG Norge, and Woodside. The authors would also like to thank Bradford Prather, Matthew Malkowski, Associate Editor Andrea Fildani, and Science Editor Shanaka de Silva for their insightful comments and helpful suggestions to improve the manuscript, and Zobe Jobe and Bradford Prather for use of original graphics adapted in Figure 1.

REFERENCES CITED

Adeogba, A.A., McHargue, T.R., and Graham, S.A., 2005, Transient fan architecture and depositional controls from near-surface 3-D seismic data, Niger Delta continental slope: AAPG Bulletin, v. 89, p. 627–643, https://doi.org/10.1306/11200404025.

Al Ja'Aidi, O.S., McCaffrey, W.D., and Kneller, B.C., 2004, Factors influencing the deposit geometry of experimental turbidity currents: implications for sand-body architecture in confined basins, *in* Lomas, S.A., and Joseph, P., eds., Confined Turbidite Systems: Geological Society of London Special Publication 222, p. 45–58, https://doi.org/10.1144/GSL.SP.2004.222.01.04.

Allen, J.R.L., 1970, A quantitative model of climbing ripples and their cross-laminated deposits: Sedimentology, v. 14, p. 5–26, https://doi.org/10.1111/j.1365-3091.1970.tb00179.x.

Allen, J.R.L., 1984, Parallel lamination developed from upper-stage plane beds: a model based on the larger coherent structures of the turbulent boundary layer: Sedimentary Geology, v. 39, p. 227–242, https://doi.org/10.1016/0037-0738(84)90052-6.

Amy, L.A., Kneller, B.C., and McCaffrey, W.D., 2007, Facies architecture of the Grès de Peira Cava, SE France: landward stacking patterns in ponded turbiditic basins: Journal of the Geological Society, v. 164, p. 143–162, https://doi.org/10.1144/0016-76492005-019.

Armitage, D.A., Romans, B.W., Covault, J.A., and Graham, S.A., 2009, The influence of mass-transport-deposit surface topography on the evolution of turbidite architecture: The Sierra Contreras, Tres Pasos Formation (Cretaceous), southern Chile: Journal of Sedimentary Research, v. 79, p. 287–301, https://doi.org/10.2110/jsr.2009.035.

Baas, J.H., Best, J.L., and Peakall, J., 2011, Depositional processes, bedform development and hybrid bed formation in rapidly decelerated cohesive (mud–sand) sediment flows: Sedimentology, v. 58, p. 1953–1987, https://doi.org/10.1111/j.1365-3091.2011.01247.x.

Baas, J.H., Best, J.L., and Peakall, J., 2016, Predicting bedforms and primary current stratification in cohesive mixtures of mud and sand: Journal of the Geological Society, v. 173, p. 12–45, https://doi.org/10.1144/jgs2015-024.

Badalini, G., Kneller, B., and Winker, C.D., 2000, Architecture and processes in the late Pleistocene Brazos-Trinity turbidite system, Gulf of Mexico continental slope, *in* Weimer, P., Slatt, R.M., Coleman, J., Rosen, N.C., Nelson, H., Bouma, A.H., Styzen, M.J., and Lawrence, D.T., eds., Deep-Water Reservoirs of the World: SEPM (Society for Sedimentary Geology), Gulf Coast Section, 20th Annual Research Conference, p. 16–34.

Baines, P.G., 1984, A unified description of two-layer flow over topography: Journal of Fluid Mechanics, v. 146, p. 127–167, https://doi.org/10.1017/S0022112084001798.

Barton, M.D., 2012, Evolution of an intra-slope apron, offshore Niger Delta Slope: Impact of step geometry on apron architecture, *in* Prather, B.E., Deptuck, M.E., Mohrig, D., Van Hoorn, B., and Wynn, R.B, eds., Application of the Principles of Seismic Geomorphology to Continental-slope and Base-of-slope systems: Case Studies from Seafloor and Near-seafloor Analogues: SEPM (Society for Sedimentary Geology) Special Publication 99, p. 181–197, https://doi.org/10.2110/pec.12.99.0181.

Beaubouef, R.T., and Abreu, V., 2006, Basin 4 of the Brazos–Trinity slope system: Anatomy of the terminal portion of an intra-slope lowstand systems tract: Gulf Coast Section Association of Geological Societies/SEPM (Society for Sedimentary Geology), 56th Annual Convention, Transactions: Lafayette, Louisiana, p. 39–48.

Beaubouef, R.T., and Friedmann, S.J., 2000, High resolution seismic/sequence stratigraphic framework for the evolution of Pleistocene intra slope basins, western Gulf of Mexico: depositional models and reservoir analogs, *in* Weimer, P., Slatt, R.M., Coleman, J., Rosen, N.C., Nelson, H., Bouma, A.H., Styzen, M.J., and Lawrence, D.T., eds., Deep-Water Reservoirs of the World: Gulf Coast Section SEPM (Society for Sedimentary Geology) 20th Annual Research Conference, p. 40–60.

Belica, M.E., Tohver, E., Pisarevsky, S.A., Jourdan, F., Denyszyn, S., and George, A.D., 2017, Middle Permian paleomagnetism of the Sydney Basin, Eastern Gondwana: Testing Pangea models and the timing of the end of the Kiaman Reverse Superchron: Tectonophysics, v. 699, p. 178–198, https://doi.org/10.1016/j.tecto.2016.12.029.

Binks, R.M., and Fairhead, J.D., 1992, A plate tectonic setting for Mesozoic rifts of West and Central Africa: Tectonophysics, v. 213, p.141–151.

Bohn, C.W., Flemings, P.B., and Slingerland, R.L., 2012, Accommodation change during bypass across a late-stage fan in the shallow Auger basin, *in* Prather, B.E., Deptuck, M.E., Mohrig, D., Van Hoorn, B., and Wynn, R.B, eds., Application of the Principles of Seismic Geomorphology to Continental-Slope and Base-of-Slope Systems: Case Studies from Seafloor and Near-Seafloor Analogues: SEPM (Society for Sedimentary Geology) Special Publication 99, p. 225–242, https://doi.org/10.2110/pec.12.99.0225.

Booth, J.R., Dean, M.C., DuVernay, A.E., and Styzen, M.J., 2003, Paleo-bathymetric controls on the stratigraphic architecture and reservoir development of confined fans in the Auger Basin: central Gulf of Mexico slope: Marine and Petroleum Geology, v. 20, p. 563–586, https://doi.org/10.1016/j.marpetgeo.2003.03.008.

Bouma, A., 1962, Sedimentology of some flysch deposits: A graphic approach to facies interpretation: Amsterdam, Elsevier, 168 p.

Brooks, H.L., Hodgson, D.M., Brunt, R.L., Peakall, J., and Flint, S.S., 2018a, Exhumed lateral margins and increasing flow confinement of a submarine landslide complex: Sedimentology, v. 65, https://doi.org/10.1111/sed.12415.

Brooks, H.L., Hodgson, D.M., Brunt, R.L., Peakall, J., Hofstra, M., and Flint, S.S., 2018b, Deep-water channel-lobe transition zone dynamics: Processes and depositional architecture, an example from the Karoo Basin, South Africa: Geological Society of America Bulletin, https://doi.org/10.1130/B31714.1 (in press).

Brunt, R.L., Di Celma, C.N., Hodgson, D.M., Flint, S.S., Kavanagh, J.P., and van der Merwe, W.C., 2013a, Driving a channel through a levee when the levee is high: An outcrop example of submarine downdip entrenchment: Marine and Petroleum Geology, v. 41, p. 134–145, https://doi.org/10.1016/j.marpetgeo.2012.02.016.

Brunt, R.L., Hodgson, D.M., Flint, S.S., Pringle, J.K., Di Celma, C., Prélat, A., and Grecula, M., 2013b, Confined to unconfined: Anatomy of a base of slope succession, Karoo Basin, South

Africa: Marine and Petroleum Geology, v. 41, p. 206–221, https://doi.org/10.1016/j.marpetgeo.2012.02.007.

Bumby, A.J., and Guiraud, R., 2005, The geodynamic setting of the Phanerozoic basins of Africa: Journal of African Earth Sciences, v. 43, p. 1–12, https://doi.org/10.1016/j.jafrearsci.2005.07.016.

Burgreen, B., and Graham, S., 2014, Evolution of a deep-water lobe system in the Neogene trench-slope setting of the East Coast Basin, New Zealand: lobe stratigraphy and architecture in a weakly confined basin configuration: Marine and Petroleum Geology, v. 54, p. 1–22, https://doi.org/10.1016/j.marpetgeo.2014.02.011.

Catuneanu, O., Hancox, P.J., and Rubidge, B.S., 1998, Reciprocal flexural behaviour and contrasting stratigraphies: A new basin development model for the Karoo retroarc foreland system, South Africa: Basin Research, v. 10, p. 417–439, https://doi.org/10.1046/j.1365-2117.1998.00078.x.

Cobain, S., Peakall, J., and Hodgson, D.M., 2015, Indicators of propagation direction and relative depth in clastic injectites: Implications for laminar versus turbulent flow processes: Geological Society of America Bulletin, v. 127, p. 1816–1830, https://doi.org/10.1130/B31209.1.

Cobain, S., Hodgson, D.M., Peakall, J., and Shiers, M.N., 2017, An integrated model of clastic injectites and basin floor lobe complexes: Implications for stratigraphic trap plays: Basin Research, v. 29, p. 816–835, https://doi.org/10.1111/bre.12229.

Covault, J.A., Hubbard, S.M., Graham, S.A., Hinsch, R., and Linzer, H.G., 2009, Turbidite-reservoir architecture in complex foredeep-margin and wedge-top depocenters, Tertiary Molasse foreland basin system, Austria: Marine and Petroleum Geology, v. 26, p. 379–396.

Deptuck, M.E., Sylvester, Z., and O'Byrne, C., 2012, Pleistocene seascape evolution above a "simple" stepped slope profile—Western Niger Delta, *in* Prather, B.E., Deptuck, M.E., Mohrig, D., Van Hoorn, B., and Wynn, R.B., eds., Application of the Principles of Seismic Geomorphology to Continental-Slope and Base-of-Slope Systems: Case Studies from Seafloor and Near-Seafloor Analogues SEPM (Society for Sedimentary Geology) Special Publication 99, p. 199–222, https://doi.org/10.2110/pec.12.99.0199.

Di Celma, C., Brunt, R.L., Hodgson, D.M., Flint, S.S., and Kavanagh, J.P., 2011, Spatial and temporal evolution of a Permian submarine slope channel-levee system, Karoo Basin, South Africa: Journal of Sedimentary Research, v. 81, p. 579–599, https://doi.org/10.2110/jsr.2011.49.

Dorrell, R.M., Peakall, J., Sumner, E.J., Parsons, D.R., Darby, S.E., Wynn, R.B., Özsoy, E., and Tezcan, D., 2016, Flow dynamics and mixing processes in hydraulic jump arrays: Implications for channel-lobe transition zones: Marine Geology, v. 381, p. 181–193, https://doi.org/10.1016/j.margeo.2016.09.009.

Doughty-Jones, G., Mayall, M., and Lonergan, L., 2017, Stratigraphy, facies and evolution of deep-water lobe complexes within a salt-controlled intra-slope minibasin: AAPG Bulletin, v. 101, p. 1879–1904, https://doi.org/10.1306/01111716046.

Edwards, D.A., Leeder, M.R., Best, J.L., and Pantin, H.M., 1994, On experimental reflected density currents and the interpretation of certain turbidites: Sedimentology, v. 41, p. 437–461, https://doi.org/10.1111/j.1365-3091.1994.tb02005.x.

Felletti, F., 2002, Complex bedding geometries and facies associations of the turbiditic fill of a confined basin in a transpressive setting (Castagnola Fm., Tertiary Piedmont Basin, NW Italy): Sedimentology, v. 49, p. 645–667, https://doi.org/10.1046/j.1365-3091.2002.00467.x.

Figueiredo, J., Hodgson, D.M., and Flint, S.S., 2010, Depositional environments and sequence stratigraphy of an exhumed Permian mud-dominated submarine slope succession, Karoo basin, South Africa: Journal of Sedimentary Research, v. 80, p. 97–118, https://doi.org/10.2110/jsr.2010.002.

Figueiredo, J.P., Hodgson, D.M., Flint, S.S., and Kavanagh, J.P., 2013, Architecture of a channel complex formed and filled during long-term degradation and entrenchment on the upper submarine slope, Unit F, Fort Brown Fm., SW Karoo Basin, South Africa: Marine and Petroleum Geology, v. 41, p. 104–116, https://doi.org/10.1016/j.marpetgeo.2012.02.006.

Flint, S.S., Hodgson, D.M., Sprague, A.R., Brunt, R.L., van der Merwe, W.C., Figueiredo, J., Prélat, A., Box, D., Di Celma, C., and Kavanagh, J.P., 2011, Depositional architecture and sequence stratigraphy of the Karoo basin floor to shelf edge succession, Laingsburg depocentre, South Africa: Marine and Petroleum Geology, v. 28, p. 658–674, https://doi.org/10.1016/j.marpetgeo.2010.06.008.

Gamberi, F., and Rovere, M., 2011, Architecture of a modern transient fan (Villafranca fan, Gioia basin-Southeastern Tyrrhenian Sea): Sedimentary Geology, v. 236, p. 211–225, https://doi.org/10.1016/j.sedgeo.2011.01.007.

García, M.H., ed., 2008, Sedimentation Engineering: Process, Measurements, Modeling and Practice: Reston, Virginia, American Society of Civil Engineers, 1150 p, https://doi.org/10.1061/9780784408148.

Grecula, M., Flint, S.S., Wickens, H.D.V., and Johnson, S.D., 2003, Upward-thickening patterns and lateral continuity of Permian sand-rich turbidite channel fills, Laingsburg Karoo, South Africa: Sedimentology, v. 50, p. 831–853, https://doi.org/10.1046/j.1365-3091.2003.00576.x.

Groenenberg, R.M., Hodgson, D.M., Prélat, A., Luthi, S.M., and Flint, S.S., 2010, Flow-deposit interaction in submarine lobes: insights from outcrop observations and realizations of a process-based numerical model: Journal of Sedimentary Research, v. 80, p. 252–267, https://doi.org/10.2110/jsr.2010.028.

Hamilton, P., Gaillot, G., Strom, K., Fedele, J., and Hoyal, D., 2017, Linking hydraulic properties in supercritical submarine distributary channels to depositional lobe geometry: Journal of Sedimentary Research, v. 87, p. 935–950, https://doi.org/10.2110/jsr.2017.53.

Haughton, P.D., 1994, Deposits of deflected and ponded turbidity currents, currents, Sorbas Basin, southeast Spain: Journal of Sedimentary Research, v. 64, p. 233–246, https://doi.org/10.1306/D4267D6B-2B26-11D7-8648000102C1865D.

Haughton, P.D., 2000, Evolving turbidite systems on a deforming basin floor, Tabernas, SE Spain: Sedimentology, v. 47, p. 497–518, https://doi.org/10.1046/j.1365-3091.2000.00293.x.

Haughton, P.D., Barker, S.P., and McCaffrey, W.D., 2003, 'Linked' debrites in sand-rich turbidite systems—origin and significance: Sedimentology, v. 50, p. 459–482, https://doi.org/10.1046/j.1365-3091.2003.00560.x.

Haughton, P., Davis, C., McCaffrey, W., and Barker, S., 2009, Hybrid sediment gravity flow deposits classification, origin and significance: Marine and Petroleum Geology, v. 26, p. 1900–1918, https://doi.org/10.1016/j.marpetgeo.2009.02.012.

Hay, D., 2012, Stratigraphic evolution of a tortuous corridor from the stepped slope of Angola, *in* Prather, B.E., Deptuck, M.E., Mohrig, D., Van Hoorn, B., and Wynn, R.B, eds., Application of the Principles of Seismic Geomorphology to Continental-Slope and Base-of-Slope Systems: Case Studies from Seafloor and Near-Seafloor Analogues SEPM (Society for Sedimentary Geology) Special Publication 99, p. 163–180, https://doi.org/10.2110/pec.12.99.0163.

Hodgson, D.M., 2009, Origin and distribution of bipartite beds in sand-rich submarine fans: Constraints from the Tanqua depocentre, Karoo Basin, South Africa: Marine and Petroleum Geology, v. 26, p. 1940–1956, https://doi.org/10.1016 /j.marpetgeo.2009.02.011.

Hodgson, D.M., and Haughton, P.D.W., 2004, Impact of syn-depositional faulting on gravity current behaviour and deep-water stratigraphy: Tabernas–Sorbas Basin, SE Spain, *in* Lomas, S., Joseph, P., eds., Confined Turbidites Systems: Geological Society of London Special Publication 222, p. 135–158, https://doi.org/10.1144/GSL.SP.2004.222.01.08.

Hodgson, D.M., Di Celma, C., Brunt, R.L., and Flint, S.S., 2011, Submarine slope degradation and aggradation and the stratigraphic evolution of channel-Levee systems: Journal of the Geological Society, v. 168, p. 625–628, https://doi.org/10.1144/0016-76492010-177.

Hodgson, D.M., Kane, I.A., Flint, S.S., Brunt, R.L., and Ortiz-Karpf, A., 2016, Time transgressive confinement on the slope and the progradation of basin-floor fans: Implications for the sequence stratigraphy of deep-water deposits: Journal of Sedimentary Research, v. 86, p. 73–86, https://doi.org/10.2110/jsr.2016.3.

Hofstra, M., Hodgson, D.M., Peakall, J., and Flint, S.S., 2015, Giant scour-fills in ancient channel-lobe transition zones: Formative processes and depositional architecture: Sedimentary Geology, v. 329, p. 98–114, https://doi.org/10.1016/j.sedgeo.2015.09.004.

Hubbard, S.M., Fildani, A., Romans, B.W., Covault, J.A., and McHargue, T.R., 2010, High-relief slope clinoform development: insights from outcrop, Magallanes Basin, Chile: Journal of Sedimentary Research, v. 80, p. 357–375, https://doi.org/10.2110/jsr.2010.042.

Ito, M., 2008, Downfan transformation from turbidity currents to debris flows at a channel-to-lobe transitional zone: The Lower Pleistocene Otadai Formation Boso Peninsula, Japan: Journal of Sedimentary Research, v. 78, p. 668–682, https://doi.org/10.2110/jsr.2008.076.

Jackson, C.A.-L., Barber, G.P., and Martinsen, O.J., 2008, Submarine slope morphology as a control on the development of sand-rich turbidite depositional systems: 3-D seismic analysis of the Kyrre Fm (Upper Cretaceous), Maloy Slope, offshore Norway: Marine and Petroleum Geology, v. 25, p. 663–680, https://doi.org/10.1016/j.marpetgeo.2007.12.007.

Jobe, Z.R., Lowe, D.R., and Morris, W.R., 2012, Climbing-ripple successions in turbidite systems: depositional environments, sedimentation rates and accumulation times: Sedimentology, v. 59, p. 867–898, https://doi.org/10.1111/j.1365-3091.2011.01283.x.

Jobe, Z.R., Sylvester, Z., Howes, N., Pirmez, C., Parker, A., Cantelli, A., Smith, R., Wolinksy, M.A., O'Byrne, C., Slowey, N., and Prather, B., 2017, High-resolution, millennial-scale patterns of bed compensation on a sand-rich intraslope submarine fan, western Niger Delta slope: Geological Society of America Bulletin, v. 129, p. 23–37, https://doi.org/10.1130/B31440.1.

Johnson, M.R., Van Vuuren, C.J., Visser, J.N.J., Cole, D.I., Wickens, H.D.V., Christie, A.D.M., and Roberts, D.L., 1997, The Foreland Karoo Basin, South Africa, *in* Selly, R.C., ed., African Basins: Sedimentary Basins of the World, v. 3: Amsterdam, Elsevier Science, p. 269–317, https://doi.org/10.1016/S1874-5997(97)80015-9.

Jones, G.E.D., Hodgson, D.M., and Flint, S.S., 2015, Lateral variability in clinoform trajectory, process regime, and sediment dispersal patterns beyond the shelf-edge rollover in exhumed basin margin-scale clinothems: Basin Research, v. 27, p. 657–680, https://doi.org/10.1111/bre.12092.

Kane, I.A., and Hodgson, D.M., 2011, Sedimentological criteria to differentiate submarine channel levee subenvironments: Exhumed examples from the Rosario Fm. (Upper Cretaceous) of Baja California, Mexico, and the Fort Brown Fm. (Permian), Karoo Basin, S. Africa: Marine and Petroleum Geology, v. 28, p. 807–823, https://doi.org/10.1016/j.marpetgeo.2010.05.009.

Kane, I.A., McCaffrey, W.D., and Peakall, J., 2008, Controls on sinuosity evolution within submarine channels: Geology, v. 36, p. 287–290, https://doi.org/10.1130/G24588A.1.

Kane, I.A., Catterall, V., McCaffrey, W.D., and Martinsen, O.J., 2010, Submarine channel response to intrabasinal tectonics: The influence of lateral tilt: AAPG Bulletin, v. 94, p. 189–219, https://doi.org/10.1306/08180909059.

Kneller, B., 1995, Beyond the turbidite paradigm: Physical models for deposition of turbidites and their implications for reservoir prediction, *in* Hartley, A.J., and Prosser, D.J., eds., Characterization of Deep Marine Clastic Systems: Geological Society of London Special Publication 94, p. 31–49, https://doi.org/10.1144/GSL.SP.1995.094.01.04.

Kneller, B., and Buckee, C., 2000, The structure and fluid mechanics of turbidity currents: a review of some recent studies and their geological implications: Sedimentology, v. 47, p. 62–94, https://doi.org/10.1046/j.1365-3091.2000.047s1062.x.

Kneller, B., and McCaffrey, W., 1999, Depositional effects of flow nonuniformity and stratification within turbidity currents approaching a bounding slope: deflection, reflection, and facies variation: Journal of Sedimentary Research, v. 69, p. 980–991, https://doi.org/10.2110/jsr.69.980.

Kneller, B.C., and Branney, M.J., 1995, Sustained high-density turbidity currents and the deposition of thick massive sands: Sedimentology, v. 42, p. 607–616, https://doi.org/10.1111/j.1365-3091.1995.tb00395.x.

Kostic, S., and Parker, G., 2006, The response of turbidity currents to a canyon-fan transition: internal hydraulic jumps and depositional signatures: Journal of Hydraulic Research, v. 44, p. 631–653, https://doi.org/10.1080/00221686.2006.9521713.

Lindeque, A., de Wit, M.J., Ryberg, T., Weber, M., and Chevallier, L., 2011, Deep crustal profile across the southern Karoo Basin and Beattie Magnetic Anomaly, South Africa: An integrated interpretation with tectonic implications: South African Journal of Geology, v. 114, p. 265–292, https://doi.org/10.2113/gssajg.114.3-4.265.

Lowe, D.R., 1982, Sediment gravity flows, II: Depositional models with special reference to the deposits of high-density turbidity currents: Journal of Sedimentary Petrology, v. 52, p. 279–298.

Lowe, D.R., 1988, Suspended-load fallout rate as an independent variable in the analysis of current structures: Sedimentology, v. 35, p. 765–776, https://doi.org/10.1111/j.1365-3091.1988.tb01250.x.

Macdonald, H.A., Wynn, R.B., Huvenne, V.A., Peakall, J., Masson, D.G., Weaver, P.P., and McPhail, S.D., 2011a, New insights into the morphology, fill, and remarkable longevity (>0.2 m.y.) of modern deep-water erosional scours along the northeast Atlantic margin: Geosphere, v. 7, p. 845–867, https://doi.org/10.1130/GES00611.1.

Macdonald, H.A., Peakall, J., Wignall, P.B., and Best, J., 2011b, Sedimentation in deep-sea lobe-elements: implications for the origin of thickening-upward sequences: Journal of the Geological Society, v. 168, p. 319–332, https://doi.org/10.1144/0016-76492010-036.

Madof, A.S., Christie-Blick, N., and Anders, M.H., 2009, Stratigraphic controls on a salt-withdrawal intraslope minibasin, north-central Green Canyon, Gulf of Mexico: Implications for misinterpreting sea level change: The American Association of Petroleum Geologists Bulletin, v. 93, p. 535–561, https://doi.org/10.1306/12220808082.

Marini, M., Milli, S., Ravnås, R., and Moscatelli, M., 2015, A comparative study of confined vs. semi-confined turbidite lobes from the Lower Messinian Laga Basin (Central Apennines, Italy): Implications for assessment of reservoir architecture: Marine and Petroleum Geology, v. 63, p. 142–165, https://doi.org/10.1016/j.marpetgeo.2015.02.015.

Marini, M., Patacci, M., Felletti, F., and McCaffrey, W.D., 2016, Fill to spill stratigraphic evolution of a confined turbidite mini-basin succession, and its likely well bore expression: The Castagnola Fm, NW Italy: Marine and Petroleum Geology, v. 69, p. 94–111, https://doi.org/10.1016/j.marpetgeo.2015.10.014.

Mayall, M., Jones, E., and Casey, M., 2006, Turbidite channel reservoirs—Key elements in facies prediction and effective development: Marine and Petroleum Geology, v. 23, p. 821–841, https://doi.org/10.1016/j.marpetgeo.2006.08.001.

Mayall, M., Lonergan, L., Bowman, A., James, S., Mills, K., Primmer, T., Pope, D., Rogers, L., and Skeene, R., 2010, The response of turbidite slope channels to growth-induced seabed topography: AAPG Bulletin, v. 94, p. 1011–1030, https://doi.org/10.1306/01051009117.

Meckel, L.D., III, Ugueto, G.A., Lynch, D.H., Hewett, B.M., Bocage, E.J., Winker, C.D., and O'Neill, B.J., 2002, Genetic stratigraphy, stratigraphic architecture, and reservoir stacking patterns of the upper Miocene–lower Pliocene greater Mars-Ursa intraslope basin, Mississippi Canyon, Gulf of Mexico, *in* Armentrout, J.M., and Rosen, N.C., eds., Sequence Stratigraphic Models for Exploration and Production: Evolving Methodology, Emerging Models, and Application Histories: GCSSEPM (Gulf Coast Section, Society for Sedimentary Geology) Foundation 22nd Annual Bob F. Perkins Research Conference Proceedings, p. 113–147.

Moody, J.D., Pyles, D.R., Clark, J., and Bouroullec, R., 2012, Quantitative outcrop characterization of an analog to weakly confined submarine channel systems: Morillo 1 member, Ainsa Basin, Spain: AAPG Bulletin, v. 96, p. 1813–1841, https://doi.org/10.1306/01061211072.

Morris, E.A., Hodgson, D.M., Brunt, R.L., and Flint, S.S., 2014a, Origin, evolution and anatomy of silt-prone submarine external levees: Sedimentology, v. 61, p. 1734–1763, https://doi.org/10.1111/sed.12114.

Morris, E.A., Hodgson, D.M., Flint, S.S., Brunt, R.L., Butterworth, P.J., and Verhaeghe, J., 2014b, Sedimentology, stratigraphic architecture, and depositional context of submarine frontal-lobe complexes: Journal of Sedimentary Research, v. 84, p. 763–780, https://doi.org/10.2110/jsr.2014.61.

Morris, E.A., Hodgson, D.M., Flint, S., Brunt, R.L., Luthi, S.M., and Kolenberg, Y., 2016, Integrating outcrop and subsurface data to assess the temporal evolution of a submarine channel–levee system: AAPG Bulletin, v. 100, p. 1663–1691, https://doi.org/10.1306/04271615056.

Mulder, T., and Alexander, J., 2001, The physical character of subaqueous sedimentary density flows and their deposits: Sedimentology, v. 48, p. 269–299, https://doi.org/10.1046/j.1365-3091.2001.00360.x.

Mutti, E., 1985, Systems and their relations to depositional sequences, *in* Zuffa, G.G., ed., Provenance of Arenites: Interpreting Provenance Relations from Detrital Modes of Sandstones: NATO-ASI Series 148: Dordrecht, D. Reidel, p. 65–93, https://doi.org/10.1007/978-94-017-2809-6_4.

Mutti, E., 1992, Turbidite Sandstones: Agip, Istituto di geologia, Università di Parma, Italy, p. 275.

Mutti, E., and Normark, W.R., 1987, Comparing examples of modern and ancient turbidite systems: Problems and concepts, *in* Leggett, J.K., and Zuffa, G.G., eds., Marine Clastic Sedimentology: Concepts and Case Studies: Dordrecht, Springer, p. 1–38, https://doi.org/10.1007/978-94-009-3241-8_1.

Mutti, E., and Normark, W.R., 1991, An integrated approach to the study of turbidite systems, *in* Weimer, P., and Link, M.H., eds., Seismic Facies and Sedimentary Processes of Submarine Fans and Turbidite Systems: New York, Springer-Verlag, p. 75–106, https://doi.org/10.1007/978-1-4684-8276-8_4.

Nasr-Azadani, M.M., and Meiburg, E., 2014, Turbidity currents interacting with three-dimensional seafloor topography: Journal of Fluid Mechanics, v. 745, p. 409–443, https://doi.org/10.1017/jfm.2014.47.

O'Byrne, C.J., Prather, B.E., Steffens, G.S., and Pirmez, C., 2004, Reservoir architectural styles across stepped slope profiles: Implications for exploration, appraisal and development [abs.]: American Association of Petroleum Geologists, International Conference and Exhibition, Cancún, Mexico, 24–27 October 2004, Abstracts CD.

Olafiranye, K., Jackson, C.A.L., and Hodgson, D.M., 2013, The role of tectonics and mass-transport complex emplacement on upper slope stratigraphic evolution: A 3-D seismic case study from offshore Angola: Marine and Petroleum Geology, v. 44, p. 196–216, https://doi.org/10.1016/j.marpetgeo.2013.02.016.

Oluboyo, A.P., Gawthorpe, R.L., Bakke, K., and Hadler-Jacobsen, F., 2014, Salt tectonic controls on deep-water turbidite depositional systems: Miocene, southwestern Lower Congo Basin, offshore Angola: Basin Research, v. 26, p. 597–620, https://doi.org/10.1111/bre.12051.

Patacci, M., Haughton, P.D., and McCaffrey, W.D., 2014, Rheological complexity in sediment gravity flows forced to decelerate against a confining slope, Braux, SE France: Journal of Sedimentary Research, v. 84, p. 270–277, https://doi.org/10.2110/jsr.2014.26.

Pemberton, E.A., Hubbard, S.M., Fildani, A., Romans, B., and Stright, L., 2016, The stratigraphic expression of decreasing confinement along a deep-water sediment routing system: Out-

crop example from southern Chile: Geosphere, v. 12, p. 114–134, https://doi.org/10.1130/GES01233.1.
Pierce, C.S., Haughton, P.D., Shannon, P.M., Pulham, A.J., Barker, S.P., and Martinsen, O.J., 2018, Variable character and diverse origin of hybrid event beds in a sandy submarine fan system, Pennsylvanian Ross Sandstone Formation, western Ireland: Sedimentology, v. 65, p. 952–992, https://doi.org/10.1111/sed.12412.
Pirmez, C., Beaubouef, R.T., Friedmann, S.J., and Mohrig, D.C., 2000, Equilibrium profile and baselevel in submarine channels: Examples from Late Pleistocene Systems and Implications for the Architecture of Deepwater Reservoir, *in* Weimer, P., Slatt, R.M., Coleman, J., Rosen, N.C., Nelson, H., Bouma, A.H., Styzen, M.J., and Lawrence, D.T., eds., GCSSEPM (Gulf Coast Section, Society for Sedimentary Geology) Foundation 20th Annual Research Conference Deep-Water Reservoirs of the Word, Houston, p. 782–805.
Pirmez, C., Prather, B.E., Mallarino, G., O'Hayer, W.W., Droxler, A.W., and Winker, C.D., 2012, Chronostratigraphy of the Brazos-Trinity depositional system, western Gulf of Mexico: Implications for deepwater depositional models, *in* Prather, B.E., Deptuck, M.E., Mohrig, D., Van Hoorn, B., and Wynn, R.B, eds., Application of the Principles of Seismic Geomorphology to Continental-Slope and Base-of-Slope Systems: Case Studies from Seafloor and Near-Seafloor Analogues: SEPM (Society for Sedimentary Geology) Special Publication 99, p.111–143, https://doi.org/10.2110/pec.12.99.0111.
Plink-Björklund, P., and Steel, R., 2002, Sea-level fall below the shelf edge, without basin-floor fans: Geology, v. 30, p. 115–118, https://doi.org/10.1130/0091-7613(2002)030<0115:SLFBTS>2.0.CO;2.
Poyatos-Moré, M., Jones, G.D., Brunt, R.L., Hodgson, D.M., Wild, R.J., and Flint, S.S., 2016, Mud-dominated basin-margin progradation: processes and implications: Journal of Sedimentary Research, v. 86, p. 863–878, https://doi.org/10.2110/jsr.2016.57.
Prather, B.E., 2000, Calibration and visualization of depositional process models for above-grade slopes: a case study from the Gulf of Mexico: Marine and Petroleum Geology, v. 17, p. 619–638, https://doi.org/10.1016/S0264-8172(00)00015-5.
Prather, B.E., 2003, Controls on reservoir distribution, architecture and stratigraphic trapping in slope settings: Marine and Petroleum Geology, v. 20, p. 529–545, https://doi.org/10.1016/j.marpetgeo.2003.03.009.
Prather, B.E., Booth, J.R., Steffens, G.S., and Craig, P.A., 1998, Classification, lithologic calibration, and stratigraphic succession of seismic facies of intraslope basins, deep-water Gulf of Mexico: AAPG Bulletin, v. 82, p. 701–728.
Prather, B.E., Pirmez, C., Sylvester, Z., and Prather, D.S., 2012a, Stratigraphic response to evolving geomorphology in a submarine apron perched on the upper Niger Delta slope, *in* Prather, B.E., Deptuck, M.E., Mohrig, D., Van Hoorn, B., and Wynn, R.B, eds., Application of the Principles of Seismic Geomorphology to Continental-Slope and Base-of-Slope Systems: Case Studies from Seafloor and Near-Seafloor Analogues: SEPM (Society for Sedimentary Geology) Special Publication 99, p. 145–161, doi:10.2110/pec.12.99.0145.
Prather, B.E., Pirmez, C., and Winker, C.D., 2012b, Stratigraphy of linked intraslope basins: Brazos-Trinity system western Gulf of Mexico, *in* Prather, B.E., Deptuck, M.E., Mohrig, D., Van Hoorn, B. and Wynn, R.B, eds., Application of the Principles of Seismic Geomorphology to Continental-Slope and Base-of-Slope Systems: Case Studies from Seafloor and Near-Seafloor Analogues: SEPM (Society for Sedimentary Geology) Special Publication 99, p. 83–109, https://doi.org/10.2110/pec.12.99.0083.
Prather, B.E., O'Byrne, C., Pirmez, C., and Sylvester, Z., 2017, Sediment partitioning, continental slopes and base-of-slope systems: Basin Research, v. 29, p. 394–416, https://doi.org/10.1111/bre.12190.
Prélat, A., and Hodgson, D.M., 2013, The full range of turbidite bed thickness patterns in submarine lobes: controls and implications: Journal of the Geological Society, v. 170, p. 209–214, https://doi.org/10.1144/jgs2012-056.
Prélat, A., Hodgson, D.M., and Flint, S.S., 2009, Evolution, architecture and hierarchy of distributary deep-water deposits: a high-resolution outcrop investigation from the Permian Karoo Basin, South Africa: Sedimentology, v. 56, p. 2132–2154, https://doi.org/10.1111/j.1365-3091.2009.01073.x.
Prélat, A., Covault, J.A., Hodgson, D.M., Fildani, A., and Flint, S.S., 2010, Intrinsic controls on the range of volumes, morphologies, and dimensions of submarine lobe: Sedimentary Geology, v. 232, p. 66–76, https://doi.org/10.1016/j.sedgeo.2010.09.010.
Raudkivi, A.J., 1976, Loose Boundary Hydraulics: Rotterdam, Pergamon Press, 397 p.
Romans, B.W., Fildani, A., Hubbard, S.M., Covault, J.A., Fosdick, J.C., and Graham, S.A., 2011, Evolution of deep-water stratigraphic architecture, Magallanes Basin, Chile: Marine and Petroleum Geology, v. 28, p. 612–628, https://doi.org/10.1016/j.marpetgeo.2010.05.002.
Rozman, D.J., 2000, Characterization of a fine-grained outer submarine fan deposit, Tanqua-Karoo Basin, South Africa, *in* Bouma, A.H., and Stone, C.G., eds., Fine-Grained Turbidite Systems: AAPG Memoir 72 and SEPM (Society for Sedimentary Geology) Special Publication 68, p. 279–290.
Saller, A.H., Noah, J.T., Ruzuar, A.P., and Schneider, R., 2004, Linked lowstand delta to basin-floor fan deposition, offshore Indonesia: An analog for deep-water reservoir systems: AAPG Bulletin, v. 88, p. 21–46, https://doi.org/10.1306/09030303003.
Salles, L., Ford, M., and Joseph, P., 2014, Characteristics of axially-sourced turbidite sedimentation on an active wedge-top basin (Annot Sandstone, SE France): Marine and Petroleum Geology, v. 56, p. 305–323, https://doi.org/10.1016/j.marpetgeo.2014.01.020.
Satterfield, W.M., and Behrens, E.W., 1990, A Late Quaternary Canyon/Channel System, Northwest Gulf of Mexico Continental Slope: Marine Geology, v. 92, p. 51–67, https://doi.org/10.1016/0025-3227(90)90026-G.
Shultz, M.R., and Hubbard, S.M., 2005, Sedimentology, stratigraphic architecture, and ichnology of gravity-flow deposits partially ponded in a growth-fault-controlled slope minibasin, Tres Pasos Formation (Cretaceous), southern Chile: Journal of Sedimentary Research, v. 75, p. 440–453, https://doi.org/10.2110/jsr.2005.034.
Sinclair, H.D., and Tomasso, M., 2002, Depositional evolution of confined turbidite basins: Journal of Sedimentary Research, v. 72, p. 451–456, https://doi.org/10.1306/111501720451.
Sixsmith, P.J., Flint, S.S., Wickens, H.D., and Johnson, S.D., 2004, Anatomy and stratigraphic development of a basin floor turbidite system in the Laingsburg Formation, main Karoo Basin, South Africa: Journal of Sedimentary Research, v. 74, p. 239–254, https://doi.org/10.1306/082903740239.
Smith, R., 2004a, Silled sub-basins to connected tortuous corridors: Sediment distribution systems on topographically complex sub-aqueous slopes, *in* Lomas, S.A., and Joseph, P., eds., Confined Turbidite Systems: Geological Society of London Special Publication 222, p. 23–43, https://doi.org/10.1144/GSL.SP.2004.222.01.03.
Smith, R., 2004b, Turbidite systems influenced by structurally induced topography in the multi-sourced Welsh Basin, *in* Lomas, S.A., and Joseph, P., eds., Confined Turbidite Systems: Geological Society of London Special Publication 222, p. 209–228, https://doi.org/10.1144/GSL.SP.2004.222.01.11.
Southern, S.J., Patacci, M., Felletti, F., and McCaffrey, W.D., 2015, Influence of flow containment and substrate entrainment upon sandy hybrid event beds containing a co-genetic mud-clast-rich division: Sedimentary Geology, v. 321, p. 105–122, https://doi.org/10.1016/j.sedgeo.2015.03.006.
Spikings, A.L., Hodgson, D.M., Paton, D.A., and Spychala, Y.T., 2015, Palinspastic restoration of an exhumed deepwater system: A workflow to improve paleogeographic reconstructions: Interpretation (Tulsa), v. 3, p. SAA71–SAA87, https://doi.org/10.1190/INT-2015-0015.1.
Spychala, Y.T., Hodgson, D.M., Flint, S.S., and Mountney, N.P., 2015, Constraining the sedimentology and stratigraphy of submarine intraslope lobe deposits using exhumed examples from the Karoo Basin, South Africa: Sedimentary Geology, v. 322, p. 67–81, https://doi.org/10.1016/j.sedgeo.2015.03.013.
Spychala, Y.T., Hodgson, D.M., Stevenson, C.J., and Flint, S.S., 2017a, Aggradational lobe fringes: The influence of subtle intrabasinal seabed topography on sediment gravity flow processes and lobe stacking patterns: Sedimentology, v. 64, p. 582–608, https://doi.org/10.1111/sed.12315.
Spychala, Y.T., Hodgson, D.M., Prélat, A., Kane, I.A., Flint, S.S., and Mountney, N.P., 2017b, Frontal and lateral submarine lobe fringes: Comparing sedimentary facies, architecture and flow processes: Journal of Sedimentary Research, v. 87, p. 75–96, https://doi.org/10.2110/jsr.2017.2.
Stevenson, C.J., Talling, P.J., Wynn, R.B., Masson, D.G., Hunt, J.E., Frenz, M., Akhmetzhanhov, A., and Cronin, B.T., 2013, The flows that left no trace: Very large-volume turbidity currents that bypassed sediment through submarine channels without eroding the sea floor: Marine and Petroleum Geology, v. 41, p. 186–205, https://doi.org/10.1016/j.marpetgeo.2012.02.008.
Stevenson, C.J., Talling, P.J., Masson, D.G., Sumner, E.J., Frenz, M., and Wynn, R.B., 2014, The spatial and temporal distribution of grain-size breaks in turbidites: Sedimentology, v. 61, p. 1120–1156, https://doi.org/10.1111/sed.12091.
Stevenson, C.J., Jackson, C.A.-L., Hodgson, D.M., Hubbard, S.M., and Eggenhuisen, J., 2015, Sediment bypass in deep-water systems: Journal of Sedimentary Research, v. 85, p. 1058–1081, https://doi.org/10.2110/jsr.2015.63.
Stow, D.A.V., and Bowen, A.J., 1980, A physical model for the transport and sorting of fine-grained sediment by turbidity currents: Sedimentology, v. 27, p. 31–46, https://doi.org/10.1111/j.1365-3091.1980.tb01156.x.

Stow, D.A.V., and Johansson, M., 2000, Deep-water massive sands: Nature, origin and hydrocarbon implications: Marine and Petroleum Geology, v. 17, p. 145–174, https://doi.org/10.1016/S0264-8172(99)00051-3.

Sumner, E.J., Peakall, J., Parsons, D.R., Wynn, R.B., Darby, S.E., Dorrell, R.M., McPhail, S.D., Perrett, J., Webb, A., and White, D., 2013, First direct measurements of hydraulic jumps in an active submarine density current: Geophysical Research Letters, v. 40, p. 5904–5908, https://doi.org/10.1002/2013GL057862.

Sylvester, Z., Cantelli, A., and Pirmez, C., 2015, Stratigraphic evolution of intraslope minibasins: Insights from surface-based model: AAPG Bulletin, v. 99, p. 1099–1129, https://doi.org/10.1306/01081514082.

Talling, P.J., 2013, Hybrid submarine flows comprising turbidity current and cohesive debris flow: Deposits, theoretical and experimental analyses, and generalized models: Geosphere, v. 9, p. 460–488, https://doi.org/10.1130/GES00793.1.

Talling, P.J., Amy, L.A., Wynn, R.B., Peakall, J., and Robinson, M., 2004, Beds comprising debrite sandwiched within co-genetic turbidite: origin and widespread occurrence in distal depositional environments: Sedimentology, v. 51, p. 163–194, https://doi.org/10.1111/j.1365-3091.2004.00617.x.

Talling, P.J., Masson, D.G., Sumner, E.J., and Malgesini, G., 2012, Subaqueous sediment density flows: Depositional processes and deposit types: Sedimentology, v. 59, p. 1937–2003, https://doi.org/10.1111/j.1365-3091.2012.01353.x.

Tankard, A., Welsink, H., Aukes, P., Newton, R., and Stettler, E., 2009, Tectonic evolution of the Cape and Karoo basins of South Africa: Marine and Petroleum Geology, v. 26, p. 1379–1412, https://doi.org/10.1016/j.marpetgeo.2009.01.022.

Van der Merwe, W.C., Flint, S.S., and Hodgson, D.M., 2010, Sequence stratigraphy of an argillaceous, deepwater basin plain succession: Vischkuil Formation (Permian), Karoo Basin, South Africa: Marine and Petroleum Geology, v. 27, p. 321–333, https://doi.org/10.1016/j.marpetgeo.2009.10.007.

Van der Merwe, W.C., Hodgson, D.M., Brunt, R.L., and Flint, S.S., 2014, Depositional architecture of sand-attached and sand-detached channel-lobe transition zones on an exhumed stepped slope mapped over a 2500 km^2 area: Geosphere, v. 10, p. 1076–1093, https://doi.org/10.1130/GES01035.1.

van der Werff, W., and Johnson, S., 2003, High resolution stratigraphic analysis of a turbidite system, Tanqua Karoo Basin, South Africa: Marine and Petroleum Geology, v. 20, p. 45–69, https://doi.org/10.1016/S0264-8172(03)00025-4.

Viljoen, J.H.A., 1992, Lithostratigraphy of the Collingham Formation (Ecca Group), including the Zoutkloof, Buffels river and Wilgenhout river members and the Matjiesfontein chert bed: Geological Survey, South African Committee for Stratigraphy, Lithostratigraphic Series, no. 22, 10 p.

Viljoen, J.H.A., 1994, Sedimentology of the Collingham Formation, Karoo Supergroup: South African Journal of Geology, v. 97, p. 167–183.

Visser, J.N.J., 1992, Basin tectonics in southwestern Gondwana during the Carboniferous and Permian, *in* de Wit, M.J., and Ransome, I.G.D., eds., Inversion Tectonics of the Cape Fold Belt, Karoo and Cretaceous Basins of Southern Africa: Rotterdam, Balkema, p. 109–116.

Visser, J.N.J., 1997, Deglaciation sequences in the Permo-Carboniferous Karoo and Kalahari basins of southern Africa: a tool in the analysis of cyclic glaciomarine basin fills: Sedimentology, v. 44, p. 507–521, https://doi.org/10.1046/j.1365-3091.1997.d01-35.x.

Visser, J.N.J., and Prackelt, H.E., 1996, Subduction, mega-shear systems and Late Palaeozoic basin development in the African segment of Gondwana: Geologische Rundschau, v. 85, p. 632–646, https://doi.org/10.1007/BF02440101.

Weckmann, U., Jung, A., Branch, T., and Ritter, O., 2007, Comparison of electrical conductivity structures and 2D magnetic modelling along two profiles crossing the Beattie Magnetic Anomaly, South Africa: South African Journal of Geology, v. 110, p. 449–464, https://doi.org/10.2113/gssajg.110.2-3.449.

Weimer, P., and Link, M.H., 1991, Global petroleum occurrences in submarine fans and turbidite systems, *in* Weimer et al., eds., Seismic Facies and Sedimentary Processes of Submarine Fans and Turbidite Systems: New York, Springer, p. 9–67, https://doi.org/10.1007/978-1-4684-8276-8_2.

Weirich, F.H., 1989, The generation of turbidity currents by subaerial debris flows, California: Geological Society of America Bulletin, v. 101, p. 278–291, https://doi.org/10.1130/0016-7606(1989)101<0278:TGOTCB>2.3.CO;2.

Winker, C.D., and Booth, J.R., 2000, Sedimentary dynamics of the salt-dominated continental slope, Gulf of Mexico: Integration of observations from the seafloor, near-surface, and deep subsurface, *in* Weimer, P., Slatt, R.M., Coleman, J., Rosen, N.C., Nelson, H., Bouma, A.H., Styzen, M.J., and Lawrence, D.T., eds., Deep-Water Reservoirs of the World: The GCSSEPM (Gulf Coast Section, Society for Sedimentary Geology) Foundation 20th Annual Bob F. Perkins Research Conference Proceedings, p. 1059–1086.

Wynn, R.B., Kenyon, N.H., Stow, D.A.V., Masson, D.G., and Weaver, P.P.E., 2002, Characterization and recognition of deep-water channel-lobe transition zones: The American Association of Petroleum Geologists Bulletin, v. 86, p. 1441–1462.